Automatic Detection of Underground Objects in Ground Penetrating Radar Images using Machine Learning

by

Leila Carolina Martoni Amaral

A thesis submitted in partial fulfillment of the requirements for the degree of

Master of Science
in
Civil (Cross-Disciplinary)

Department of Civil and Environmental Engineering
University of Alberta

Abstract

The population increase has stimulated the need for the creation and expansion of existing urban infrastructures such as sewer, water, power and telecommunication lines. In order to support this need, multiple efforts to find sustainable solutions that support the urbanization trend have been studied. As a solution, construction methods such as trenchless techniques—ranging from maxi horizontal directional drilling for large-scale pipe installations to microtrenching for the installation of telecommunications infrastructure, that offer reduced social and environmental impacts compared to conventional opencut construction methods, are becoming more accessible and increasingly used. Despite the advantages of underground construction, challenges exist in knowing the locations of existing subsurface utilities or other underground objects (such as rocks) an that uncertainty can impact new installations. Existing non-destructive technologies, such as ground penetrating radar (GPR), can be used to map extensive areas in a fast and accurate manner and support the construction of new infrastructure. However, GPR data is difficult to interpret, and requires an experienced person to be able to locate the features within the image that correspond to objects. In order to overcome the issue of data interpretation, multiple studies aiming towards the automation of GPR data interpretation have been conducted—however, the methods proposed can still improve in terms of detection speed and accuracy.

The objective of this research is to automate GPR data interpretation to support underground construction. To achieve this, an extensive database of GPR images due to commonly encountered underground objects, such as rock-sized boulders and PVC and metal pipes, was collected based on GPR measurements in a laboratory setting. The database compiled from these measurements was used alongside different machine learning algorithms, including YOLO v3 and R-CNN, to determine the methodology that has higher accuracy of detection and classification for the

automated object detection based on the correspondent features in GPR images. The limitations of the various algorithms are considered, and recommendations are proposed for future studies.

A study on the long-term performance evaluation of micro-trenching backfill materials was continued, with GPR surveys performed to precisely determine conduit depth within the micro-trench. Updated measurements of conduit depth were compared to previously collected data to determine the conduit displacement four to seven years after installation.

Preface

This paper-based thesis is an original work by Leila Carolina Martoni Amaral under the supervision of Dr. Alireza Bayat. Part of the research project, of which this thesis is a part, has been submitted for publication as journal papers.

Chapter 2: **Review of Machine Learning Algorithms for Automatic Detection of Underground Objects in GPR Images**, has been accepted for publication with minor reviews in the American Society of Civil Engineers (ASCE) *Journal of Pipeline Systems Engineering and Practice*. The literature review was conducted by me under the supervision of Dr. Ali Bayat. Dr. Aditya Roshan and Dr. Ali Bayat both participated in the manuscript organization and provided oversight of the work.

Chapter 3: **Automatic Detection and Classification of Underground Objects in Ground Penetrating Radar (GPR) Images using Deep Learning**. Dr. Aditya Roshan and I were responsible for data collection. I was responsible for writing the paper, data interpretation and preparation for the implementation of the machine learning algorithms. The machine learning algorithms were done jointly with Dr. Aditya Roshan. Dr. Ali Bayat and Aditya Roshan participated in the concept formation and manuscript organization.

Chapter 4: **Long-term GPR Monitoring of the Performance of Materials used as Backfill for Micro-Trenching in Cold Climates** it is being formatted to be submitted for publication with the *International Journal of Pavement Research and Technology*. Dr. Aditya Roshan and I were responsible for data collection. I was responsible for data processing and interpretation, as well as manuscript creation. Dr. Ali Bayat provided oversight of the work and was involved with the concept formation and with review of the results.

Dedicated to

God, who gave me strength and guided me throughout my academic journey.

My parents, for providing spiritual and emotional support.

Matt for the good humor and support during difficult times.

I couldn’t have done this without them.

Acknowledgments

I would like to express my deep gratitude and sincere appreciation to my supervisor, Dr. Ali Bayat for being so understanding while supporting and encouraging me during academic courses, thesis completion and life after university. Dr. Bayat is an amazing person and an inspiration for me as a professional.

My gratitude is also extended to Lana Gutwin who supported me throughout the master's journey by always being available for a talk, constantly guiding me in the best direction, and for the review of all my work and assistance with the papers submitted for publication.

I also would like to thank all my research group colleagues for sharing great moments and knowledge at our office. I would like to especially thank my colleague Zahra, who always supported me throughout my academic and personal struggles, Aditya for the assistance in performing laboratory and field data collection and for all patient in passing his broad knowledge of machine learning, and Thomas Johnson for guiding me on how to perform GPR data collection.

Table of Contents

List of Tables

List of Figures

1. Introduction

Rapid population increase worldwide has impacted the way that urban infrastructure is being developed and what technologies are being used during construction to reduce social and environmental impacts (Figure 1-1). For example, Alberta is projected to have an increase of two million people from 2019 to 2046 (Treasury Board and Finance 2020). In order to adapt to the needs of this growing population, underground construction is necessary to guaranty quality of life by ensuring availability of water, sewer, gas, electricity, and telecommunications infrastructure.

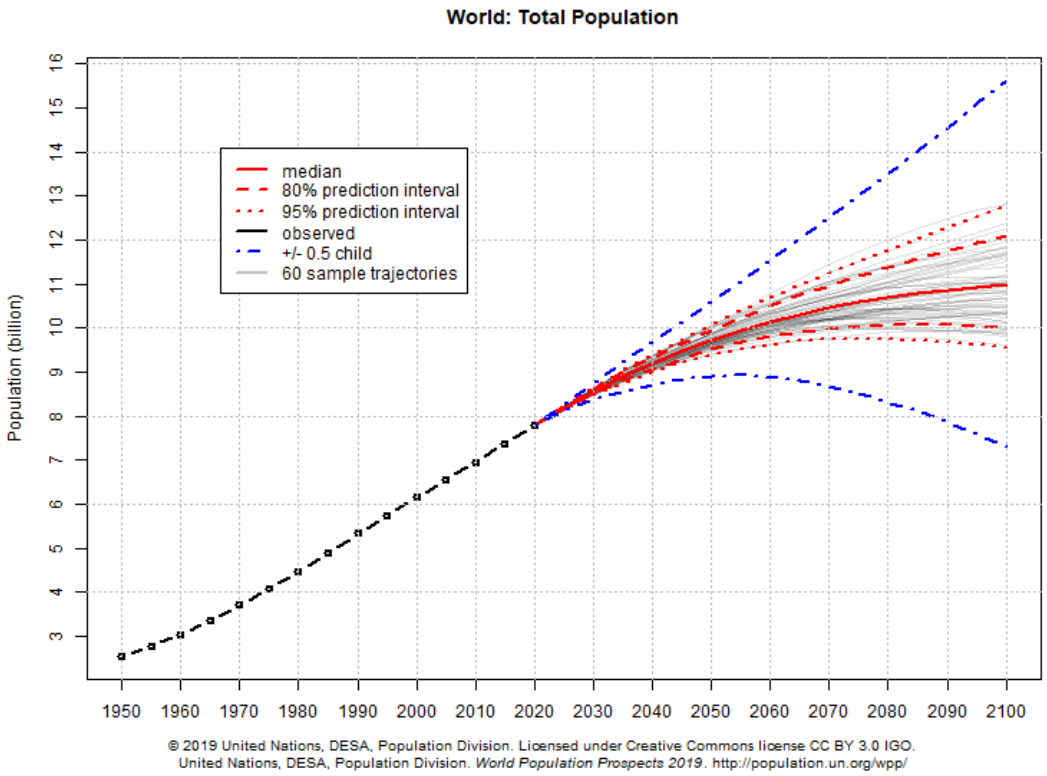

Figure 1-1: Population estimate and probabilistic projections (United Nations 2019)

In the past, underground infrastructure construction and repair were done utilizing open-cut methods; however, the increase in costs related to traffic and business disruption, surface restoration, the necessity of excavating around existing utilities, traffic delay and increase in environmental regulations (when crossing wetlands and rivers) resulted in the gradual substitution of open-cut methods with trenchless construction methods (Allouche et al. 2000). For trenchless projects to be successful, extensive subsurface diagnosis—including characterization of soil and geological formations and determination of the location of existing infrastructure—is extremely important. When the subsurface is not adequately investigated, unforeseen events can impact

design and construction, by damaging drilling equipment, impacting borehole path design, damaging existing utilities (increasing construction cost and causing delays) and causing incidents that compromise safety (worker injuries and/or explosions when hitting a gas line or electric cable, for example) (Moganti 2016).

An alternative to support the increasing demand for subsurface utilities such as telecommunication transmission lines is the use of micro-trenching. Micro-trenching (MT) installations are done by marking a path, cutting a small trench, cleaning the trench, placing the conduit (which contains the fibre), followed by application of backfill and sealant. In contrast to other trenchless projects, MT installations are usually performed in asphalt or sidewalks and thus at a shallower depth. Due to the shallow depth of the installation, the risks related to micro-trenching projects are different than for trenchless projects in general, and much of the risk is dependent on the material used to backfill the trench.

In order to support applications such as trenchless construction and performance evaluation of micro-trenching, ground penetrating radar (GPR) has been widely used. GPR is a non-destructive geophysical tool capable of locating subsurface objects in a fast and accurate manner (Liu et al. 2002). Even with the known benefits, GPR data interpretation remains a challenge due to the complexity of data analysis and the time required. Recent efforts have been made to apply machine learning to the automation of GPR data interpretation, but the lack of available training data and algorithm generalization capabilities are topics that still need attention.

1.1. Objective

The object of this research is to assess the capabilities of machine learning in the automation of underground object detection based on GPR images and to build on previous studies that used GPR technology for the long-term performance evaluation of MT backfill materials. For this purpose, the following research problems were addressed:

- Understand previously used methodologies for the automatic detection of underground objects based on GPR images
- Establish a training dataset of GPR images collected under controlled (laboratory) conditions, including images of pipes, voids and boulders in a sand medium

- Implement a fast and accurate machine learning methodology to identify and classify underground objects based on GPR images
- Apply existing GPR methods to monitor an existing MT pilot installation

1.2. Methodology

This research was conducted in three phases: literature review, implementation of ML to automatically detect and identify features in GPR images corresponding to underground objects and apply GPR to the long-term performance monitoring of a pilot micro-trenching installation. In the first phase, existing methods and resources for automated interpretation of GPR images were compiled—including algorithms, data pre-processing and training data sets. This comprehensive literature review supported the identification of accurate and fast ML algorithms that were applied in the second phase of research. The second phase involved the creation of a database of GPR images of underground objects that was used to assess the capabilities of YOLO v3 and R-CNN to automate GPR image interpretation. The third phase consisted in the visual assessment of MT conditions and application of GPR to determine conduit depth for a series of pilot MT installations. The acquired measurements were compared to measurements from previous years to determine current conduit displacement.

1.3. Thesis Structure

This paper-based thesis is organized into five chapters, each of which is briefly described below.

Chapter 1: *Introduction*

In this chapter, the research topic, motivations of the research, objectives, methodology, and thesis structure are presented.

Chapter 2: *Review of Machine Learning Algorithms for Automatic Detection of Underground Objects in GPR Images*

In this chapter, a deep review of previously used methodologies and algorithms to automatically detect and identify features in GPR images corresponding to underground objects is presented and discussed. The steps used during the automatic detection process (including pre-processing, post-processing), algorithm choice and capabilities, and data used for training and testing algorithms

are presented and compared. Important factors for the success of the implementation of automatic detection of objects based on GPR images, such as data availability, are discussed.

Chapter 3: *Automatic Underground Object Detection and Classification based on Ground Penetrating Radar Images using Deep Learning*

In this chapter, the results of testing of two deep learning algorithms—YOLO v3 and R-CNN—to automate GPR data interpretation are presented. The algorithms were trained and tested using GPR images collected in a laboratory setting. Commonly encountered underground objects, including pipes, boulders and voids, were buried in a sand box to represent real world scenarios. GPR data collection was performed on these known objects to create an extensive database used for training and validations of the ML models.

Chapter 4: *Long-Term Performance Monitoring of Backfill Materials for Microtrenching in Cold Climates using Ground Penetrating Radar*

In this chapter, the capabilities of GPR for monitoring the long-term performance of MT was tested in a pilot installation. A GPR survey was performed to locate the fibre-optic cables and to determine cable depth. Cable displacement was determined by comparing current cable depth and depths determined from GPR surveys conducted in previous years. The observed cable displacements for the backfill material used in each section of the micro-trench were used to assess the performance of the backfill material at the time of the survey.

Chapter 5: *Summary and Conclusions*

In this chapter, the capabilities of GPR in locating objects that may impact trenchless construction are investigated and summarized. The limitations of the current work and future research are also discussed.

2. Review of Machine Learning Algorithms for Automatic Detection of Underground Objects in GPR Images

2.1. Abstract

Ground penetrating radar is a non-destructive tool that has gained popularity after giving promising results in different areas, such as utility engineering, transportation engineering, civil engineering, and geology, with relatively low cost. Even as the number of applications for GPR increases, the interpretation of GPR data is still challenging, in part due to varying ground conditions. Researchers are continuously working on the development of new analysis methods to address these challenges. Computer vision algorithms, including neural networks and convolution neural networks, have advanced significantly over the past decade, and researchers have utilized these algorithms to extract information from GPR images and thus improve interpretation of GPR data. This paper presents a review of literature that employs computer vision and machine learning algorithms, such YOLO v3, Viola Jones and AlexNet, for automatic extraction of information from GPR images. The uptake in use of automatic detection algorithms for GPR is increased by the ability to rapidly quantify and locate buried targets that previously could only be identified by professionals with a high level of expertise and training.

2.2. Introduction

Ground penetrating radar (GPR) is non-destructive electromagnetic geophysical technique that offers remarkable advantages compared to other non-destructive testing. The benefits of GPR include equipment portability, relatively low cost and high versatility, allowing it to be applied in different fields of study, such as utility engineering, transportation engineering, civil engineering, archeology, and geology (Travassos and Pantoja 2019). By varying the frequency of electromagnetic waves, GPR can be used to map the shallow subsurface and indicate the depth and location of buried objects. Unforeseen circumstances are often encountered during underground construction work or trenchless construction, including adverse events such as machinery damage from encountering an obstacle or low productivity rates due to boulders/cobbles. Such risk events inevitably result in negative impacts on the cost and schedule of a project. However, it is possible to reduce the risk of encountering underground obstacles along the excavation path by identifying and locating them in advance. Examples of underground objects

that can be detected by GPR are utility lines (e.g., electrical, water, sewage, gas, and telecommunications lines) or objects such as rocks, boulders and cobbles, and rebar (Figure 2-1).

Figure 2-1: GPR signal response showing the similarity of GPR reflections for objects of different materials

Even with the advantages of GPR, the complexity of the resulting signal remains an issue. An experienced person is often needed to process complex GPR data using advanced software to enhance target reflections and reduce noise. Depending on the signal quality and the area surveyed, this process can be time consuming, and is also subject to human error (Hall et al. 2002; Saarenketo and Scullion, 2000; Shihab et al. 2002; Zhang et al. 2020).

Different approaches for automatic detection and interpretation systems for GPR data have been proposed and applied successfully (Shihab et al. 2002); however, existing methods can still improve in terms of accuracy, rapidity, and efficiency of detection. This paper presents an overview of the different methods used for automated detection and interpretation of GPR signals from 1995 to 2020, including Hough transform, template matching, edge detection, thresholding, and machine learning methods, along with comparisons of the various methods. In studying the different algorithms, the primary objective is to identify methods that reduce the effort consumed during the pre-processing and processing of GPR data, while at the same time increasing accuracy.

2.3. Automatic Object Detection using GPR

The time required to analyze GPR images and the complexity of the process have incentivized the use of automatic object detection. Automatic object detection involves identifying the location of

an object (i.e., the area with a high probability of detecting an object) and the object category, in a fast and accurate manner (Zhao et al. 2019). Areas with high probabilities are marked with a bounding box, and each box corresponds to a certain class or type of object. Two major approaches have been used, classical image processing and machine learning (ML) based image processing (including artificial neural networks (ANN)). While classical image processing methods are brute force methods and require high computational resources, ANNs are promising, processing information in a way that is analogous to how human brain would function (Macukow 2016).

The first attempt to use ANN was by McCulloch and Pitts in 1943. They developed a simple neural network (NN) using electrical circuits to describe how neurons in the brain might work (McCulloch and Pitts 1943). According to Stancu et al. (2018) the development of neural networks can be divided into five stages: 1) beginning of neural networks, 2) golden age, 3) quiet years, 4) years of renewed enthusiasm, and 5) permanent development. At present, with the availability of high computing power, machine learning and neural networks are continuously evolving.

With the permanent development in artificial intelligence (AI), deep learning (DL)—a ML method based on ANN—has gained significant attention, as it produces faster and more accurate results (Ertam and Aydın 2017). Rapid advances in DL have enabled the creation of robust tools capable of solving existing problems in classical image processing by improving network architecture, training strategies, and optimization functions (Zhao et al. 2019).

2.3.1. 1990s: Early Introduction of NN for Processing GPR Images

The first article applying NN to analysis of GPR data was published in 1995, during the years of renewed enthusiasm for NN. The authors proposed a methodology to detect rebar and its size and depth using a three-layer fully connected ANN with backpropagation for training purposes (Molyneaux et al. 1995). Backpropagation is a commonly used ANN training algorithm that is capable of recognizing complex patterns; however, it requires a long processing time (Avan et al. 2017). Experimental data was collected in a tank filled with an oil-water emulsion (to mimic concrete, which has similar dielectric property) containing rebar and voids. This controlled setup gives better data than a GPR survey conducted in the real world, since concrete contains aggregates and has variations in the internal moisture content. The results of the study demonstrated the capability of the NN to identify the position and depth of rebar, but not its size. Overall, this

introductory study was a big step in the use of ANN for automatic detection of GPR object reflections, showing the promising future of this approach.

2.3.2. Classical Approaches for GPR Image Processing

During the period of renewed enthusiasm for NN, other methodologies were applied to automate detection of objects in GPR data. One of the most widely used algorithms in visual pattern recognition of lines, ellipses, and hyperbolas was the classical Hough transform (HT) algorithm (Basak and Das 2003) first introduced by Duda and Hart in 1972. The original HT algorithm has been improved over the years, generating modified versions such as generalized HT and randomized HT (Köppen et al. 2001). HT algorithms (and other image processing algorithms) require input parameters, such as threshold values for bright pixels and selection of regions of interest in the image.

In 1998, Capineri proposed a real-time approach, based on HT, for line and hyperbola detection in GPR images, giving information about the position size and shape of buried objects (e.g., water pipes, sewage ducts, and electrical and gas networks) (Capineri et al. 1998). According to Capineri (1998), an ideal program would be automated, but this requires additional computational time. The use of HT in Capineri's methodology resulted in detection with less than 7% error in pipe position and less than 2% error in pipe location. However, all HT methods (classical and improved) are brute force methods and require high computational capacity to be practical. At the time, manual steps were included in the methodology in order to minimize these issues (Capineri et al. 1998).

Even after renewed enthusiasm with the advance of NN in GPR detection, classical methods were still being utilized. One example is a paper by Al-Nuaimy et al. that proposed edge detection (automated detection of the boundaries of the area of interest) within GPR images and enhancement techniques to reduce input data and thus overall computational time (2001). Ardekani (2006) proposed a methodology that involved pre-processing, edge detection and HT steps. (Golovko 2007) also proposed a method to locate objects within GPR images using HT. According to Kaur et al. (2016) and Khan et al. (2020), edge detection, thresholding, and template matching require manual adjustments and are known to be inadequate when GPR images are blurry due to the presence of noise and outliers; therefore, these methods are not appropriate for advanced performance in real-world situations. In addition, according to Kaur et al. (2016), the threshold

method, based on using average intensity values to detect the boundary that separates the target reflections from the background, binarizes the image, creating a fragile image representation that is dependant on the chosen threshold. In the early 2000s, NN algorithms were still evolving, and thus classical methods were still studied as a solution for image recognition problems, despite the problems mentioned. Currently, these problems have been solved using ML algorithms and therefore, ML has replaced the use of classical methods.

2.3.3. 2000s: NN and Training for GPR Images

In the early 2000s, the popularity of NN declined rapidly, due to factors such as overfitting, the requirement for high amounts of training data (and its availability), and limited computing capability (Zhao et al. 2019). The first articles that applied NN to GPR image analysis, such as Al-Nuaimy et al. (2000), focused on reducing input data in order to decrease computation time. However, these issues are being addressed due to advances in computer technology—for example, improvements in computational capabilities, including in graphical processing units (GPUs), have enabled applications that were previously not practical due to long execution times (Nickolls and Dally 2010).

In 2000, Al-Nuaimy et al. proposed a series of signal and image processing steps before application of NN in order to achieve high accuracy and resolution in locating pipes, cables, and anti-personnel landmines using GPR. The signal processing step included background noise removal, path loss compensation, antenna separation rectification and low pass filters. After signal processing, Welch-averaged overlapping periodograms were used to estimate the power of the signal at different frequencies and thus extract the regions that represented echo signals of target reflections. The selected regions were used to train the NN using backpropagation. The three-layer, fully-connected, feed-forward NN was used to analyze the radargram, indicating regions that might contain relevant reflections. Then, the identified regions were further processed using edge detection and HT to determine the location and depth of the target object. Automatic extraction of regions of interest before applying HT reduced the processing time compared to manual extraction, as in the method described by Capineri (1998).

In 2002, Shihab et al. followed previously described approaches to reduce the amount of data analyzed and lower computational processing time. To accomplish this, they proposed a

methodology in which the pre-processing step was based on statistical analysis of GPR A-scan images. The pre-processing stage applied statistical functions to differentiate object reflections and noise. To achieve this, different statistical functions were assessed, and the variance, mean, absolute deviation and fourth moment of the signal were demonstrated to enhance signal features corresponding to object reflections. After preprocessing, the next step was classification, which was done by applying a three-layer feed-forward NN. Images of pipes, tanks, voids, and rebar were used to train the NN using backpropagation. The results of the classification were indicated by highlighting the areas of the radargram that contained object reflections. The highlighted areas were further evaluated using HT to confirm the existence of objects and indicate the depth of the classified objects. Shihab et al. (2002) demonstrated that it is possible to reduce the amount of input data used in the NN step by 80% through statistical analysis of A-scans. However, multiple steps (i.e., re-evaluation of highlighted areas using HT) were required to achieve the desired results.

Youn et al. (2003) used two ANNs to identify drainage pipes buried at depths of about 60 cm in clay loam and silt loam soil. The first ANN (ANN-1) was used to search for a waveform peak (similar to those identified in the training data) in the GPR image. The second ANN (ANN-2) was used to determine whether the waveform identified by ANN-1 corresponded to a hyperbolic reflection pattern. The result of the dual ANN process was the generation of an image, including the depth and position of the pipe.

During the 2000s, GPR image analysis studies highlighted the overall strength of NN and support vector machines (SVM) (Stancu et al. 2018). SVM is a classification and regression prediction algorithm that uses ML to increase accuracy and prevent data overfitting (Jakkula 2006). SVM started to gain popularity for automatic detection in GPR images around 2004, nearly a decade after the first introduction of SVM by Vapnik in 1995 for optical character recognition (Vapnik 2000). In general, both ANNs and SVMs have been widely used for object detections in GPR images. However, Xie et al. (2013) have pointed out some defects in ANN development, such as the tendency to get trapped in a local optimum, the sensitivity of ANN to the training dataset, and the limited generalization ability of ANNs. In contrast, SVMs have good generalization capabilities, even when the training dataset is small. However, the challenge with SVM is to

determine the appropriate features—i.e., the kernel function and training parameters—to give the best results (Shao et al. 2007).

Zhang et al. (2004) adapted a methodology described by Zhang and Wong (2001), which uses linear SVM for gene selection and classification, for application to image analysis in GPR. The images used for training and classification were generated using two anti-personnel mines and a stone buried at various depths in different soils. To perform feature extraction, a linear SVM was used to maximize the separation margin, minimize the number of misclassified samples, and give better generalization when extracting the important features of the image. After this, a recursive classification and leave-one-out cross-validation was used to assess the performance of the SVM classifier. In addition, to achieve adequate classification accuracy, random permutation was used to analyze the probability of errors during the cross-validation (Zhang et al. 2004). This methodology worked well for the detection and classification of landmines using GPR images.

Even with the rise and application of new machine learning methods, NNs showed strong improvement between 2000 and 2015. This motivated development of different methodologies for the analysis of GPR images involving NN until 2015, when deep learning algorithms such as convolutional neural networks (CNNs) started to be applied to object detection using GPR images.

In 2005, Shaw et al. created a multi-layer perception (MLP) network (a class of feedforward ANN) for analysis of GPR images using the Stuttgart Neural Network Simulator (SNNS), which was trained by a resilient backpropagation (RPROP) algorithm. RPROP has achieved faster convergence and higher accuracy than original backpropagation by improvements in the learning rate (Avan et al. 2017; Prasad et al. 2013). The GPR radargrams used during the training process were collected in an oil/water emulsion tank containing rebar: the oil/water emulsion was used instead of concrete to facilitate data collection, since the emulsion has a similar dielectric value, but does not require time to mature. However, voids filled with air or water change the dielectric of a material. Any variation in compaction while pouring concrete can result in heterogeneity, and variation in the dielectric properties of the concrete. Thus, the data used to train the NN might not be representative. Before applying the MLP network, the GPR images were pre-processed using background removal to improve the visibility and detection of the hyperbolae. After that, the MLP network—comprising a single layer with eight hidden nodes—performed pattern recognition using radargrams of rebar in real concrete slabs at predetermined depths. Based on GPR data taken using

the test environment (i.e., the emulsion tank), the existence, lateral position and depth of rebar were identified by NN. However, the NN was not used successfully in identifying rebar in concrete slabs, due to signal attenuation. To summarize, while the methodology developed works for detection of hyperbolae in GPR images, training of the NN should be done using datasets collected in the same environment in which the NN is to be applied. This approach increased object accuracy by 69%.

Pasolli et al. 2008 followed four steps to achieve automatic detection and classification of underground objects based on GPR data: pre-processing, segmentation, object detection and material recognition. For pre-processing, a median filter was applied to reduce noise, a simple averaging operation was used for time zero correction, and a time gain was used to compensate for signal attenuation. In the segmentation stage, a modulus operator and Kapur's thresholding were applied. Single object detection was done using a genetic optimization algorithm (GA) which was run in cascade (i.e., the information collected from the output of the GA was used as additional information for the next classifier for each of the patterns searched) when trying to locate multiple objects. For each identified pattern, geospatial coordinates were extracted. Material recognition was done by an SVM using a radial basis function (RBF) kernel, a mathematical function that allows SVM to classify a dataset (originally in one dimension) in two-dimensions (Patle and Chouhan 2013). This approach gave an overall classification accuracy of 80% when determining the existence, position, and material of a buried object based on GPR data.

In the following year, Pasolli et al. (2009) refined the methodology, adding a fifth step to estimate the size of objects. Object dimension extraction was done using a regression approach based on Gaussian processes (GP). The methodology was tested for images generated using the open-source software gprMax (Giannopoulos 2005) based on a background of uniform sandy soil, achieving a 18% relative mean absolute error. In this case, the accuracy of the methodology was not determined, since the existence, position, and material of the buried objects were considered known.

Birkenfeld (2010) used a NN trained with trapezoidal bounded images containing half of a hyperbolic reflection (i.e., images containing the apex and one branch of a hyperbola). The training data was pre-processed using a low-pass filter, background noise removal and gain filters. A standard multilayer feed-forward network was trained using a backpropagation algorithm with the

application of receptive fields and local connections, which increases the perception of faint and distorted hyperbolas. The NN detected multiple activities areas selected based on a threshold value, and the activities areas are discretized by using a Gaussian filter to locate the highest activity point, which corresponds to the apex of the hyperbola. The algorithm is very sensitive, and, depending on the chosen threshold value, can lead to misclassifications of hyperbolic reflections within the image. One improvement recommended by Kaur et al. (2016) is that curve fitting could be applied to extract hyperbolic parameters.

2.3.4. 2010s: Advanced NN for GPR Image Processing

Kobashigawa et al. (2011) compared the performance of NN and genetic programming (GP) to automatically detect unexploded ordnance (UXO). GP, which was first introduced in 1999 by Koza et al., is a fairly new method that uses principles of Darwinian natural selection (such as crossover, mutation and reproduction) to generate computer programs to perform a given task. According to Khan et al. (2020), GP was developed to achieve optimum or near-optimum outputs to computationally difficult problems. One of the reasons that optimum solutions can be attained using GP is because sizes and structures are not defined by trial-and-error methods (as done for NN) (Kobashigawa et al. 2011). Kobashigawa et al. used FEKO (2005) to generate radargrams with different levels of noise, which were used to train a NN and GP. Four different NN structures were trained and tested, including NN structures with neurons of the backpropagation, and a radial basis, feed-forward NN. Genetic programming (GP) was performed in MATLAB and evaluated using the ratio of the number of correctly classified patterns to the total number of patterns Overall, compared to backpropagation NN, GP gave better classifications and faster performance when a high level of noise was present in the GPR image, achieving accuracies of 90 to 97%.

Maas and Schmalzl (2013) used ML to locate areas containing hyperbolic reflections on radargrams in unprocessed data in real time using the Viola-Jones algorithm (Sathya and Abraham 2013). According to the authors, training the Viola-Jones cascade classifier can take up to two weeks, depending on the settings, sample size, and resolution. After training, the algorithm can be used for automatic detection by dividing the original radargram into multiple sub-radargrams. In each sub-radargram, the search window looks for Haar-like features, i.e., features used to encode differences in average intensities between rectangular regions within an image (Mita et al. 2005). The Viola-Jones algorithm is based on *N* stages, consisting of weak classifiers called subwindows.

As the algorithm analyzes each subwindow, one at a time, and the image is either rejected or progresses to the next subwindow. If an image passes through all *N* subwindows without being rejected, an object is detected (Viola and Jones 2004). After application of the Viola-Jones algorithm, Canny edge detection and HT were applied to precisely determine the position and depth for each of the hyperbolae, as well as the signal velocity. This methodology worked well in situations with low noise and clear hyperbolic reflections; however, when reflections were noisy, hyperbolae could not be identified (Maas and Schmalzl 2013). Another factor that may have decreased the detection capability of the algorithm is the background variation in the input data compared to the training data. With the available data, this algorithm achieved an accuracy of 65 to 75%, with 7% false positives. According to Maas and Schmalzl (2013), the accuracy of this method was directly related to the amount of training data available; thus it cannot be compared to other methods.

Núñez-Nieto et al. (2014) tested logistic regressions and NNs to calculate the probability of locating landmines and UXO by GPR. GPR radargrams were collected in an experimental setting and filtered with time zero correction, dewow filtering, gain filtering and background noise removal. The images collected were sliced and used to train the logistic regression and NN algorithms. After training, the model was run, with a set of values ranging between 0 and 1 as the output. In order to determine if an object is present or not, a threshold value (between 0 and 1) must be assigned. A lower threshold value can result in an increased number of false positives. Overall, the study showed that the two NNs performed better than logistic regression for underground object location, with accuracies of 92% and 89%, respectively. The authors also suggested that more training data should be generated for different types of soils to expand the detection capabilities of the methods in different environments.

In 2015, convolutional neural networks (CNNs) (which were first introduced by LeCun et al. in 1990) started to be applied to GPR, although they were already widely used in other areas, such as character recognition (Al-Jawfi 2009; LeCun et al. 1990). Lecun et al. introduced LeNet, a simple structured CNN in 1998, which further popularized CNNs by making them easier to apply. CNNs were proven by Krizhevsky et al. 2012 to work well for difficult image recognition problems (Wang and Raj 2017).

Besaw and Stimac (2015) proposed a deep CNN to automatically identify and categorize signals in GPR images as buried explosive hazards (BEHs) or false alarms (FAs). BEHs and FAs are represented by hyperbolic signatures (similarly to utility reflections), and therefore this methodology can also be used for other GPR applications. The methodology consisted of preprocessing, anomaly detection, postprocessing, discrimination and algorithm fusion stages. During the preprocessing stage, spatial resampling, ground-bounce tracking and alignment, and A-scan phase alignment were applied to the images. This was followed by anomaly detection using a deep belief network (a class of deep NN that acts as hyperbola detectors). Images of the identified targets were further processed using a two-dimensional median filter and a zero-score component analysis (ZCA) to prepare the images used to train the CNN algorithm. The CNN for object detection and classification comprised two convolutional layers and a single layer with a fully-connected ANN. To prevent overtraining—i.e., reduction in generalization of detection—when the CNN is applied to new data, Besaw and Stimac (2015) used cross-validation, network weight regularization and dropout strategies. One of the benefits of CNN is that, compared to a standard feed-forward NN composed of layers of a similar size, it has fewer connections and parameters, and therefore it is easier to train (Hashemi 2019). The performance of the CNN was compared with a texture feature coding method (TFCM) and edge histogram descriptors (EHD) (two traditional methods for feature extraction which extract important features in an image to make the recognition task easier and more accurate). Compared to TFCM and EHD, CNN showed superior performance, achieving 72% detection accuracy, as well as fewer false alarms.

Kaur et al. (2016) applied SVM and curve fitting to GPR images for the identification of hyperbolic reflections of rebar in bridge decks. In contrast to methods proposed by previous authors (Al-Nuaimy et al. 2001; Pasolli et al. 2008), Kaur et al. avoided a pre-processing thresholding step. The SVM classifier was trained by manually labeling GPR radargrams collected on a bridge deck. SVM classifiers using different template matching and feature vectors—such as intensity values, intensity histogram, edge pixels, maximum gradient orientation, histogram of oriented gradients [HOG]—were tested. Of these classifiers, HOG features showed the best accuracy, precision, sensitivity and specificity; thus, HOG features were used to train and classify rebar reflections. The SVM classifier identified clustered regions of possible hyperbolic reflections, in which the centroid of each cluster was computed. The final step was to apply random sample consensus curve fitting (a robust curve fitting method that works well in the presence of outliers) for the selected

regions to determine the precise location of the rebar. Approximately 92% accuracy was achieved for rebar detection and hyperbola fitting.

Dou et al. (2017) proposed a method that involved pre-processing of a GPR image and application of a threshold value (automatically determined based on edge detection results) to separate target reflections from the background. According to the authors (Dou et al. 2017), the proposed classical threshold method has proved to be more efficient in separating the target reflection compared to the maximum entropy thresholding method proposed in Kapur thresholding (used by Pasolli et al. 2008), in which the resultant threshold value is too high and results in suppression of target reflections. A column-connection clustering (C3) algorithm was then applied to the previously selected regions to separate regions of interest and serve as input for a three-layer feedforward NN (trained using backpropagation). After using the NN to identify the area in which the hyperbola was located, an orthogonal distance-fitting algorithm was applied for hyperbola fitting, determining the size and depth of the object. The C3 algorithm resolved multiple overlapping hyperbolas into separated images and worked well with GPR signals containing noise. It also demonstrated high efficiency and the ability to detect hyperbolae in real-time GPR surveys (70% accuracy).

Kim et al. (2018) adopted a deep-learning object classification methodology that consisted of three steps: data collection, data pre-processing and data classification. During data collection, GPR data was acquired to build a library with statistical analyses applied to automatically determine upper and lower threshold limits for feature enhancement. The threshold amplitude limits enhanced important features in the images, such as target reflections, but also enhanced noise signals. The resultant image was cropped with a mask consisting of m x n pixels and used during a manual labeling process. After labeling, images were prepared for CNN training using AlexNet. AlexNet is a deep convolutional neural network that emerged in 2012 to fulfill a need for performance improvements when using larger datasets, such as ImageNet (Deng et al. 2009). In addition, AlexNet can learn more powerful models while preventing overfitting, i.e., when the model does not generalize well from the training data to unseen data (Krizhevsky et al. 2012). Kim et al. (2018) stated that object detection accuracy depended on the amount of training data, however, they achieved an accuracy of 98% for object classification with the available data.

In 2019, Zong et al. continued the application of deep learning aimed at classifying GPR images in real time. Training images were collected from a moving vehicle and labeled manually using categories—e.g., rainwater wells, cables, metal/non-metal pipes, and sparse/dense steel reinforcement. To improve NN detection capabilities, the collected images were augmented using an albumentations library (Buslaev et al. 2018). Albumentations libraries apply image adjustments such as random cropping, small angle rotation, blurring, etc., in order to increase existing training examples, consequently reducing overfitting (Krizhevsky et al. 2012). Zong et al. (2019) used YOLO v3 (Redmon and Farhadi 2018b) in conjunction with Darknet 53 (Redmon 2013) to classify and locate target reflections in radargrams in real time. Darknet 53— a CNN used as a foundation for object detection problems and YOLO workflows (Redmon 2013)—was trained to extract the features of the training images using convolution kernel networks. YOLO v3, a CNN that works as a single-stage detector, was used to locate target reflections in GPR images in a single pass (Valiati and Menotti 2019). Using the two CNNs (Darknet 53 and YOLO v3), the authors achieved a precision of over 85% in identifying object reflections, as well as correctly locating and classifying objects.

In 2020, Gong and Zhang applied a fast region-based convolutional neural network (Faster R-CNN) (Girshick 2015) to images generated using gprMax software (Giannopoulos 2005). Faster R-CNN is an end-to-end object detection CNN, which means it is capable of determining candidate regions of objects, as well as performing feature extraction, classification and location refinement (Gong and Zhang 2020). In order to increase the database generated with gprMax software, image manipulation techniques, such as horizontal and vertical flipping, stretching, compression, image cropping and enhancement, were applied, which increased the dataset from 40 to 200 images, improving detection capabilities. The results showed an accuracy for detection and classification of around 94%. The simulated images presented in the article showed low noise levels. In order to determine the level of accuracy in real GPR scenarios, the authors suggested that further studies should be done to increase the image dataset (Gong and Zhang 2020).

Based on the results reported by Zong et al. (2019) and Gong and Zhang (2020), YOLO v3 gives better performance (in terms of sensitivity and speed) compared to Faster R-CNN. However, a comparison of the reported accuracies indicates that both methodologies achieve similar results (Benjdira et al. 2019).

A chronological summary of the application of machine learning algorithms in GPR image processing is given in TABLE 2-1. Highlights of the outputs of the various machine learning algorithms are also summarized in the table.

TABLE 2-1: Chronological summary of application of ML algorithms in GPR image processing

Reference	Methodology	Dataset	Number of Images	Number of Classes	ML	Accuracy/Results
Molyneaux et al., 1995	(1) Collection of GPR images (2) NN trained by backpropagation algorithm (3) NN applied to GPR images	Images taken using an emulsion tank with and without rebars at varying depth	Training: 153 (99 of rebar, 54 without rebar) Testing: 132 (101 with rebar, 99 without)	Two classes: (1) rebar present, and (2) no rebar detected	NN	Overall accuracy of 82% for hyperbolic detection and correct depth classification
Al-Nuaimy et al., 2000	(1) Data preprocessed using background noise removal, path loss compensation, antenna separation rectification and low-pass filters (2) Welch-averaged overlapping periodograms of signal segments applied (3) NN trained using backpropagation (4) NN used to locate areas of object reflections; HT further applied to identify exact location and depth of targets	Radargrams of landmines and pipes of different materials	Training: 10 radargrams (8 pipes and 2 landmines) (each radargram presented in the paper had 1-3 hyperbolic reflections)	Two classes: (1) object reflection, and (2) background reflection	NN	Promising results for locating and assigning depth of pipes, cables, and anti-personnel landmines, but high computational cost
Shihab et al., 2002	(1) Statistical analysis used to reduce input data (2) NN trained using backpropagation algorithm (3) NN used to locate regions of possible object location (4) HT used to confirm existence of target and determine hyperbola parameters such as depth	Images of pipes, tanks, voids, rebars and non-targets		Two classes: (1) object reflection, and (2) background reflection	NN	Statistical analysis reduced input data by 80%. Proposed methodology can locate objects with better accuracy than a trained operator

Youn et al., 2003	Used two ANNs to (1) Locate waveform peak (similar to the ones on GPR images) (2) Determine whether waveform corresponds to a hyperbolic reflection pattern	Drainage pipes in farmlands with a variety of soil types			NN	2D map with depth and position of pipes
Zhang et al., 2004	(1) Linear SVM (2) Recursive classification, leave-one-out cross validation and random permutation assessed algorithm performance and accuracy	Non-metallic AP mines (PFM and PMN) and stones		Six classes: PFM and PMN in sand, PMN and stone in earth, Sand and earth background	SVM	Showed feasibility of feature extraction and classification of landmine images
Shaw, M. R., et al. 2005	(1) Images of rebar in emulsion tank used for training purposes (2) RBP algorithm using training images, trained multi-layer perception network (MLP) (3) MLP network identified parabolas and determined rebar depth in real reinforced concrete		Training: 388 images Testing: 390 images		NN	Accuracy of 69% for object detection (in real data detections) Depth prediction error varied between 0.7% to 47%
Pasolli et al., 2008	(1) Data preprocessing using median filter, simple average operation and time gain (2) Modulus operator and Kapur's thresholding used to segment data (3) GA using unsupervised learning used for object detection (4) SVM using RBF Kernel function applied for object material classification	Buried objects with varying position, size, shape and material type	Testing: 120 images		GA, SVM	71% accuracy for object detection; overall classification and detection of 80%

Pasolli et al. (2009)	(1) Data preprocessing using median filter, simple average operation and time gain (2) Modulus operator and Kapur's thresholding used to segment data (3) GA using unsupervised learning used for object detection (4) SVM using RBF Kernel function applied for object material classification (as in Pasolli et al., 2008) (5) Gaussian processes (GP) used for object dimension extraction (Pasolli et al., 2009)	GprMax images with varying depth, size, position and surrounding material for circular, squared and uniform layer objects	Testing: 2500		GA, SVM	Object dimension achieved 18% relative mean absolute error
Birkenfeld, 2010	(1) Data preprocessing using low-pass filter, background removal and gain filters (2) Multilayer feedforward network trained using backpropagation algorithm (3) NN used to identify areas of possible location of hyperbola apex above a threshold limit (3) Gaussian filter applied to determine apex location	Pipes and cables of different sizes and materials buried in six different soils and at varying depths	Training: 1000 images (showing the apex and one branch of hyperbola). Tested on hundreds of radargrams		NN	Algorithm is very sensitive, classifies incomplete hyperbolae reflections, but can lead to false positives depending on the chosen threshold value.
Kobashigawa et al., 2011	(1) Dataset creation using FEKO software (2) Network training using Genetic programing and NN algorithms with different architectures	Images generated in FEKO with 5 different objects and noises levels added in MATALAB	Training: 1350	Two classes: UXO and non-UXO	GP and NN	Classification accuracy varied from 90 to 97% GP showed faster classification performance than NN in images with

						high levels of noise
Maas & Schmalzl, 2013	(1) Viola-Jones algorithm used to locate areas of hyperbolic reflection in unprocessed images (2) Canny edge detector used to binarize image (3) HT extracts hyperbola parameters and signal velocity	Four datasets	Training dataset: 8005 (3020 of hyperbolas and 4985 negative sample reflections (such as background reflections)) Testing dataset: 342		Viola - Jones	Detection rates vary between 75 and 65% with a false detection rate of approximately 7% Methodology can be used for real time object detection. Training process can take up to two weeks
Núñez-Nieto et al., 2014	(1) NN and logistic regression (LR) algorithms trained with real data and tested (2) Output is a value between 0 and 1 (3) Requires selection of threshold value between 0 and 1 to characterize the existence or not of an object	Data set composed of GPR traces as input		Two classes: (1) safe regions and (2) dangerous regions	NN	NN achieved accuracy of 92%; LR achieved accuracy of 89% for object detection
Besaw & Stimac, 2015	(1) Data preprocessing using spatial resampling, ground-bounce tracking and alignment, and A-scan phase alignment (2) Deep belief network used for anomaly detection (3) 2D median filter and zero-score component analysis applied to training data (4) CNN used for object detection and classification	Database was created by collecting data in a test range with buried explosive hazards	Testing: 1800 m2 of GPR data with total of 786 unique target. (Unsupervised learning, no training data required)	Two classes: (1) buried explosive hazards and (2) false alarms	CNN	CNN had 72% accuracy, the best detection probability and the lowest rate of false alarms compared to texture feature coding method and edge histogram descriptors

Kaur et al. (2016a)	(1) SVM using HOG for classifications (2) Curve fitting done by random sample consensus	Three datasets from different bridge decks	Training: 2400 images Testing: 4000 images Cross-validation: 600 images	Two classes: Positive and negative	SVM	Rebar detection accuracy of 96% and 92% accuracy for detection and hyperbola fitting
Dou et al., 2017	(1) Thresholding (2) C3 algorithm selected regions of interest (3) Backpropagation algorithm used to train NN (3) NN applied for object detection (4) Hyperbola fitting performed using orthogonal distance		Training: 3434 images (464 real hyperbolae and 3000 negative samples)		NN	70% accuracy; can be used in real-time surveys
Kim et al., 2018	(1) Data preprocessing and feature enhancement using statistical information (2) Object detection and classification used AlexNet transfer learning		Training: 10296 images Testing: 10296 images	Four classes: (1) hyperbola, (2) manhole, (3) layer interface and (4) ground	CNN - Alex Net	Accuracy of 98% for object detection and classification. For noisy images, feature enhancement can enhance noise as well as reflections
Zong et al., 2019	(1) Original and augmented images were used for training purposes (2) Training used transfer learning from ImageNet, COCO and PASCAL VOC data sets (3) Darknet 53 CNN used to extract features of the buried objects (4) YOLO v3 used to classify and locate the objects	GPR system collected data around the city	Training: 3522 images (489 labelled and 3033 augmented)	Eight classes: (1) rainwater wells, (2) cables, (3) metal and (4) nonmetal pipes, (5) sparse	YOLO v3	Accuracy of detection and classification of 85%; Can be used in real-time surveys

				and (6) dense steel, (7) reinforce ment, and (8) voids		
Gong & Zhang, 2020	(1) Training set composed of computationally created images using gprMax (2) DA method expanded available data (3) Faster R-CNN used for object detection and classification	Dataset produced using GprMax	Training: 160 images Testing: 40 images	Three classes: rebar, and rounded and rectangle objects	Faster R-CNN	Accuracy of 94% for detection and classification

2.4. Training Data: Impact and Availability

The availability of GPR databases to train and test ML algorithms is a limiting factor in the real-world application of automatic object detection techniques. This is because automatic object detection involves more than distinguishing between target objects and non-target reflection, as done by Al-Nuaimy et al. (2000), Kaur et al. (2016), Kobashigawa et al. (2011), Molyneaux et al. (1995), and Núñez-Nieto et al. (2014). Further research (Gong & Zhang 2020; Kim et al. 2018; Jing Zhang et al. 2004; Zong et al. 2019), is underway to classify the identified targets, which increases the complexity of the problem and requires larger datasets. To solve this larger problem, a representative GPR library should include multiple images of different objects in a variety of real environments (e.g., soil conditions, depth, material, etc.), collected using different GPR systems, and with different levels of background noise. Some alternative methodologies have been used to resolve the issue of the limited training data available, such as augmentation libraries and computer-generated images (such as gprMax) but training algorithms using such images only increases detection accuracy slightly. A summary of the available data, including the size of the datasets (including the number of training, testing and cross-validation samples) is presented in Figure 2-2, which is a representation of the relationship between the number of samples in the dataset and algorithm accuracy.

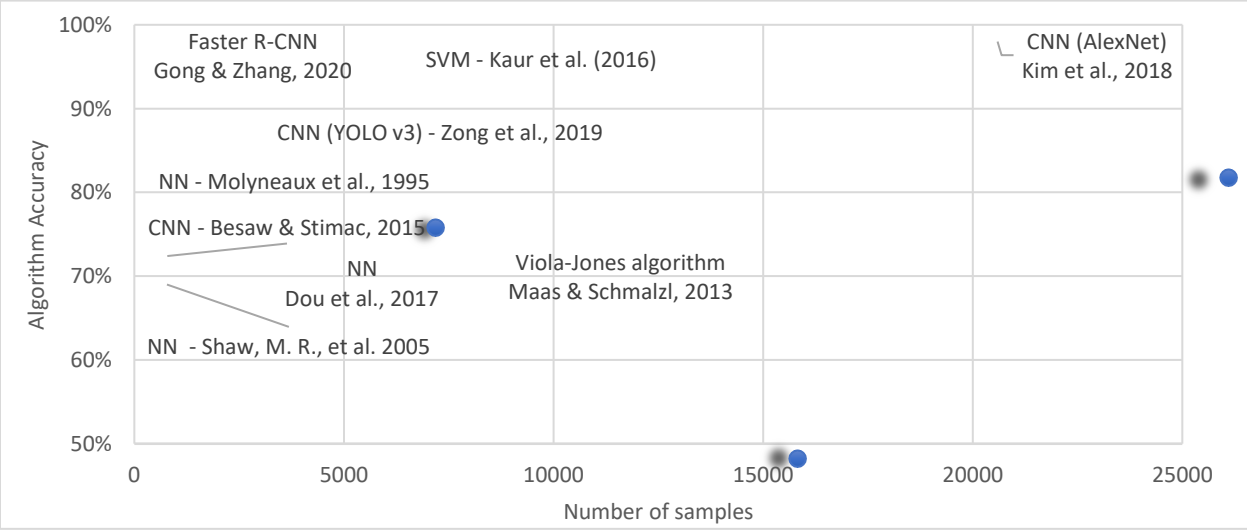

Figure 2-2: Relationship between sample size of dataset and algorithm accuracy

As seen in Figure 2-2, the AlexNet algorithm (Kim et al. 2018) trained with 20592 images resulted in an accuracy of 98%, while an SVM (Kaur et al. 2016) trained with 6400 images resulted in a

slightly lower accuracy (96%). The discrepancy between the large increase in the sample size and the small improvement in accuracy can be related to algorithm capabilities, such as generalization, but also to the level of noise in the GPR images. This may explain why some of the methodologies might have high algorithm accuracy despite having been tested in images with little or no noise present. An example of the impact of the complexity of GPR images on accuracy can be seen in the work of Maas and Schmalzl (2013). In this work, unprocessed radargrams were used, decreasing the contrast between the target reflections and background. Even with a relatively high number of training samples, this model had a lower accuracy than other models trained and tested with fewer samples. The discrepancies in GPR image characteristics makes it difficult to determine whether the capability of an algorithm to recognize and classify objects correctly can be attributed to the algorithm or to the characteristics of the images used to train and test the algorithms. If algorithms are trained with an extensive dataset, the accuracy of the results can be related to the capability of the algorithms; however, low accuracy can more often be attributed to deficiencies in the training datasets.

2.5. Conclusion

This article summarizes AI-based methodologies used to implement automatic object detection and classification of GPR images in work published between 1995 and 2020. The necessity of reducing human interpretation time and bias in the analysis of GPR data, in conjunction with the permanent development of artificial intelligence, is reflected in significant efforts to apply visual computing methods used in other applications (such as facial recognition) to locating and classifying underground objects based on GPR images. As of 2021, many different algorithm structures have been proposed, including YOLO V3, AlexNet, SVM and Viola Jones. However, finding an optimal solution is still an ongoing effort and depends somewhat on the desired output (e.g. high accuracy for object location, detection in real time, detection under specific conditions, etc.).

A high degree of time and effort is currently spent in developing GPR training data by separate research groups. The effort expended by research groups to generate representative datasets of GPR images decreases the actual time available to focus on the development of algorithms to automate interpretation. Classification of underground objects could be vastly improved if an open-source GPR library of labeled images was available for use in training algorithms, similar to

the image datasets tailored to visual computation problems (such as ImageNet (Deng et al. 2009) and COCO (Lin et al. 2014)) that are available for general use.

Even with the current deficits in training data, which generally reduce the accuracy of detection algorithms, certain ML techniques have demonstrated real-time detection and classification capabilities of up to 98% accuracy. In comparison, a trained specialist could spend months interpreting a similar dataset (depending on its size and complexity). Thus, many of the ML techniques summarized in this work show promise in facilitating the interpretation of GPR images with further development.

2.6. Data Availability Statement

No data, models, or code were generated or used during the study (e.g., opinion or data-less paper).

3. Automatic Underground Object Detection and Classification based on Ground Penetrating Radar Images using Deep Learning

3.1. Abstract

Ground penetrating radar (GPR) is a non-destructive tool that has gained popularity in supporting underground projects such as HDD, after giving promising results in subsurface mapping. Even with the benefits including equipment portability, low cost, and high versatility in locating objects, GPR has a drawback of the time spent in data interpretation. Because of this, to increase the number of radargrams analyzed in a fraction of time, multiple efforts have been made to automate data interpretation through machine learning. Recent researchers have shown success in using deep learning for automatic detection of underground objects however, GPR images variations such as the presence of noise, type of equipment used, and variety of buried objects makes it hard to find a deep learning solution with generalization capacity to detect targets in such variable conditions. This study evaluates the effectiveness of YOLO v3 and R-CNN in detecting and classifying GPR images. A 2GHz high-frequency GPR antenna was used in a laboratory setup to build a GPR dataset with images of pipes, air and water voids, and boulders. The proposed scheme successfully detected and classified underground objects feature presented in GPR images, achieving 57% and 84% f1 scores for R-CNN and YOLO v3 respectively.

Keywords: Ground Penetrating Radar, Machine learning, YOLO v3, and R-CNN.

3.2. Introduction

The rapid growth of urban areas has increased the need to expand underground infrastructures by creating new and/or reconstructing existing utilities such as water, sewer, gas, and fiber-optic lines. The success of new underground construction relies on the understanding of existing subsurface structures. The presence of impediments—such as boulder-sized rocks or any other objects that are difficult to penetrate or that can complicate, be hazardous, and damage the equipment when digging, trenching, or boring— need to be located in advance to the beginning of construction (Young and Alft 2004). Studies have shown that accurate subsurface mapping increases safety and productivity by minimizing the risks related to hitting existing utilities, (such as gas lines), increases design reliability by working the design of new utilities around existing ones, increases the precision of cost estimation by accounting for any needed utility relocates, and decreases the

possibility of delays, claims, change orders, or damage costs due to public injury or utility damage, etc. (Arcand et al. 2006).

To facilitate greater understanding of subsurface utility distribution, many efforts have been made related to urban data management. Those efforts include the creation of a geographic information system (GIS) integrated database to share information on new and existing utilities (Cazzaniga et al. 2013). However, there are limitations associated with such databases. Subsurface databases often contain incomplete or low-accuracy data (Cazzaniga et al. 2013), and they also lack information regarding other objects, such as rocks.

Ground penetrating radar (GPR) is a non-destructive geophysical technique that offers remarkable advantages, including portability, low survey cost, low initial investment, the ability to cover large areas, and versatility (Travassos and Pantoja 2019). GPR provides excellent resolution (except in highly conductive environments, such as clay soils) in locating underground utilities and other underground objects, such as rocks. GPR can achieve a quality level B (QL-B) in utility locates, the "designating" level, which is the second highest level of accuracy, just under the highest level QL-A (ASCE 2002).

3.3. Principles of GPR

GPR works by sending out an electromagnetic signal and recording the time that takes for a receiver to capture the signal energy that is reflected from the subsurface. The reflected energy varies according to the dielectric property of the subsurface material that the electromagnetic (EM) signal travels through. The EM velocity change at the boundaries between materials with different properties and also reflects the characteristic of the target object (e.g., material, size). For example, the output of a typical GPR survey is an image called B-scan, which shows hyperbolic reflections for cylindrical or rounded targets (such as pipe cross-sections or rocks) and linear reflections, representing layers and pipe extensions. To interpret B-scan images, a series of processing steps are necessary to reduce noise and signal attenuation (the loss of energy that occurs by energy absorption as the signal travels through the medium), making the contrasts between the target object and background material more evident.

The complexity involved with GPR data analysis requires an experienced person to interpret GPR data and therefore to identify target reflections. In addition to the presence of noise and signal

attenuation, the sheer size of the datasets collected can increase the time required for data analysis, increasing the overall cost of GPR (Bianchini Ciampoli et al. 2019). In addition, the analysis of a variety of GPR images over extended hours can decrease the efficiency in visually recognizing important information, and therefore decreasing the possibility of detecting target objects (Vejdannik et al. 2018).

3.3.1. GPR Data Interpretation

In the real world, images can be visualized in color (red-green-blue or RGB), and it reproduces the real characteristics of an object or person. On the other hand, GPR images infer object characteristics such as shape and material by registering the amplitude variation of the EM signal. GPR images are usually visualized in greyscale, and the intensity of the reflection is represented by brighter or lighter reflections. The strength of a reflection is proportional to the difference in dielectric constant (a property of the object) between two distinct materials, and the higher the difference in dielectric, the brighter the reflection (GSSI 2016). An example of good contrast can be observed in Figure 3-1, where a metal pipe gives a brighter reflection than a boulder or PVC pipe. Moreover, the difference in the PVC and boulder reflections can be seen by the pattern change (also called reflection polarity), in which the dominant band (brighter reflection) and the halo effect represent the change in the signal velocity. For the PVC pipe, since the PVC pipe was filled with air, the EM signal passed from soil to air, with the velocity of the signal increasing when it reached the air to generate a negative reflection (black/white/black). The opposite effect occurs when the EM signal hits the boulder and the velocity of the signal slows down, resulting in a white/black/white reflection (Figure 3-1) (GSSI 2016).

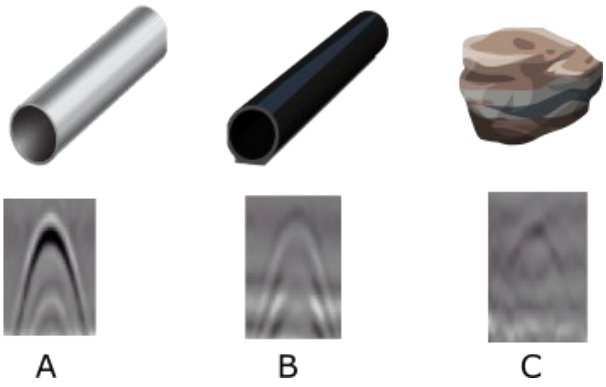

Figure 3-1: GPR images from (A) a metal pipe, (B), a PVC pipe and (C) a boulder

3.4. Machine Learning for Automatic Object Detection

ML has already been widely used to automate a variety of tasks, such as facial recognition, object detection and localization, image characterization and activity recognition (Dhillon and Verma 2020). It can perform tasks beyond human capabilities when it involve the processing of large and complex datasets (Alzubi et al. 2018). When comparing to human ability to perform GPR object detection, ML can achieve higher accuracy, higher detection speed, and lower cost. In addition, existing algorithms, such as YOLO v3, can be used in near real-time and real-time applications, which can support new technologies such as HDD GPR equipped bore-head, to avoid hitting objects during drilling in real time (Manacorda et al. 2014).

3.4.1. Background of ML in GPR Automatic Object Detection

The first effort to solve the problem of the time required for the analysis of GPR images was in 1995, when Molyneaux et al. (1995) applied neural networks (NN) to automatically detect reflections for rebar in concrete (and determine the size and depth of the rebar). At first, NN and classical approaches such as Hough transform (HT) (Capineri et al. 1998), edge detection (Al-Nuaimy et al. 2001) and thresholding (Ardekani 2006) were used to automate object detection. However, these methods required manual inputs and eventually were overtaken by ML techniques such as deep learning (DL). Lately, DL has been applied widely, not only for automatic detection of object reflections in GPR images, but also for the automatic classification of the identified objects. Promising results have been achieved for several different algorithms, for instance: AlexNet achieved 98% accuracy in object classification based on real GPR images (Kim et al. 2018);, real GPR images that were further augmented were used to train and test Darknet 53 and YOLO v3, achieving 89% accuracy in detection and classification (Zong et al. 2019); and augmented computer-generated images were used to test and train a Faster R-CNN algorithm, with 94% accuracy achieved for detection and classification (Gong and Zhang 2020).

The successful application of a variety of supervised ML algorithms, such as YOLO v3 and R-CNN family, arises from the algorithm's ability to learn from a dataset of labeled images, enabling the identification of objects in unlabeled data. To accurately identify and classify objects in images, an extensive labeled dataset is required for model training. A variety of images of common objects used for training of object recognition algorithms —including vehicles, animals, people, household items, etc.—are available online in labeled datasets such as ImageNet (Deng et al. 2009), Microsoft

COCO (Lin et al. 2014), and PASCAL VOC (Everingham et al. 2010). However, a similar online database of GPR images suitable for training datasets, containing images captured using different GPR equipment, with background noise, and images collected in a variety of subsurface conditions, with buried objects of different types, materials and sizes is not available. Even while a variety of papers related to the automatic detection of objects in GPR images are available, only a few researchers such as Dérobert and Pajewski (2018), have made GPR image databases available. In addition to the time-consuming task of collecting GPR data, images need to be carefully labeled by experts, which makes the process of forming a reliable database expensive and time-consuming (Huang et al. 2020). In addition to limited data availability, another challenge in ML is the algorithm generalization capacity. This term refers to the capability of an algorithm to generalize detection of features in images that were not included in the training dataset. The generalization capacity of an algorithm decreases in cases where there are limited training images available for a variety of conditions.

Overall, the current goals for the automatic detection of objects in GPR images are the creation of a database with a variety of images, to be used in an algorithm with good generalization capabilities. This involves achieving high detection and classification speed and accuracy, so that the method can possibly be used for real-time applications.

3.5. R-CNN and YOLO v3

The main objective of this research is to compare and evaluate the object detection models R-CNN and YOLO v3 to determine the best algorithm that best performs classification and detection of object features in GPR images.

R-CNN (Region-based Convolutional Neural Networks - Girshick et al. 2014) is a multistage algorithm that works by using a selective search to generate regions of interest (ROI) (i.e., candidate object locations), which are used as input in a CNN, that acts as a feature extractor, and its output is used by an SVM (support vector machine) to classify and assign, using a bounding box regression, object detection results. The drawback of this algorithm is the multistage training (i.e., training involves multiple steps, including object proposal for 2000 regions, object detection and bounding box learning) which makes the process expensive in terms of computational space and time (Girshick 2015). In addition to the considerations about training, object detection relies

on a region proposal for each object within the image, which makes the overall process slow, and consumes massive data, time and computational effort (Du 2018).

YOLO (You Only Look Once) v3 is a fully CNN capable of performing end-to-end detection—i.e. the algorithm can detect and classify images in one step, which includes the prediction of bounding boxes and the class prediction probability for each bounding box (Redmon and Farhadi 2018a). YOLO v3 divides the input image into grids, that if the ground truth falls into a grid, that grid will detect, predict, and classify the object using bounding boxes. YOLO v3 is faster than R-CNN because it uses logistic regression, for object detection, allowing object location and category to be predicted at the same time (Huang et al. 2020; Redmon and Farhadi 2018a). Even with the benefit of fast detection from YOLO v3, the group of Region-Based CNN (R-CNN, Fast R-CNN, and Faster R-CNN) can achieve better accuracy than YOLO v3.

R-CNN and YOLO v3 used TensorFlow as a framework and VGG-16 (visual geometry group - a CNN model with 13 convolutional layers and 3 fully connected layers) as a feature extractor. VGG-16 was pre-trained using ImageNet (Deng et al. 2009).

3.5.1. Experimental Data Collection and Dataset Creation

The dataset used to train and test the algorithm was formed of GPR images collected using a GSSI-SIR 4000 GPR unit (Geophysical Survey Systems, Inc.) coupled with a 2000 MHz palm antenna (GSSI – Model 62000). Data collection was performed using a laboratory set-up comprising a large plastic bin (dimensions 1.3 x 1.3 x 0.4m) filled with homogeneous dry sandy soil. Five different target objects were used, including lengths of metal and plastic pipe, boulder, and air-filled and water-filled balloons (to represent air and water voids) (Figure 3-2).

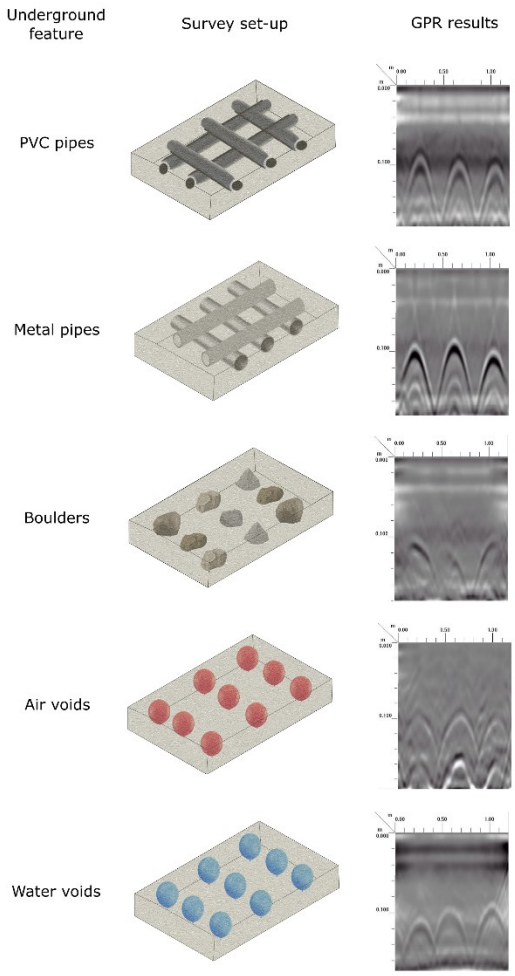

Figure 3-2: GPR survey setup and resulting GPR images

The GPR image data set generated using the laboratory setup contains a total of 352 images, of which were divided in 80% for training and for 20% for model validation using the Pareto Principle. The labeled dataset was created using LabelImg (an open-source graphical image notation tool), in which annotations retrieved from manually assigned object bounding boxes in the images generated XML files containing the category of the object, the coordinates of the bounding box, and the size and depth of the image (Figure 3-3).

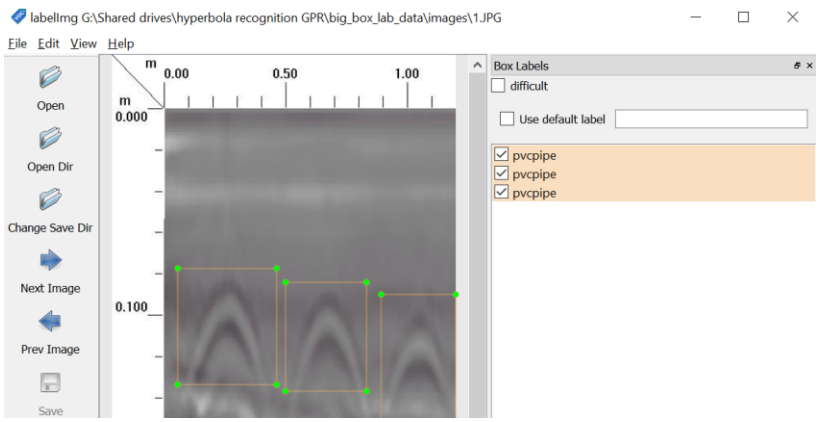

Figure 3-3: GPR image labeling process

3.6. Experimental Results and Analysis

The results of R-CNN and YOLO v3 for feature detection in GPR images are shown in Figure 3-4 and Figure 3-5.

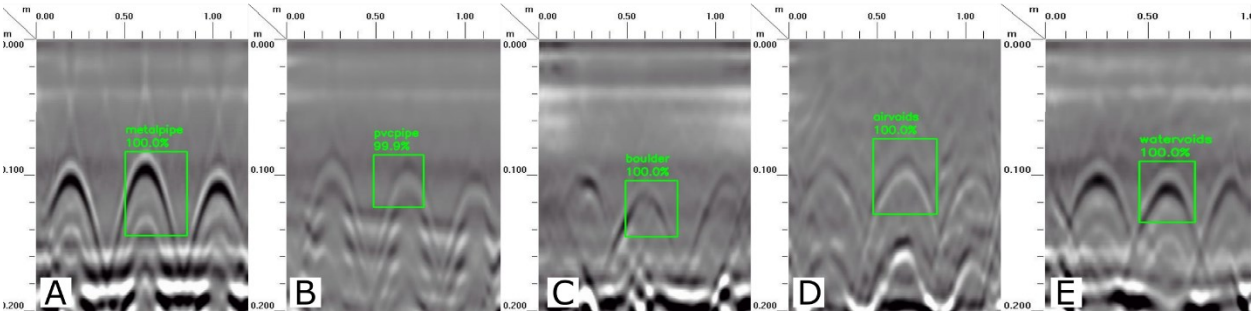

Figure 3-4: R-CNN results for metal pipes (A), PVC pipes (B), boulders (C), air voids (D) and water voids (E)

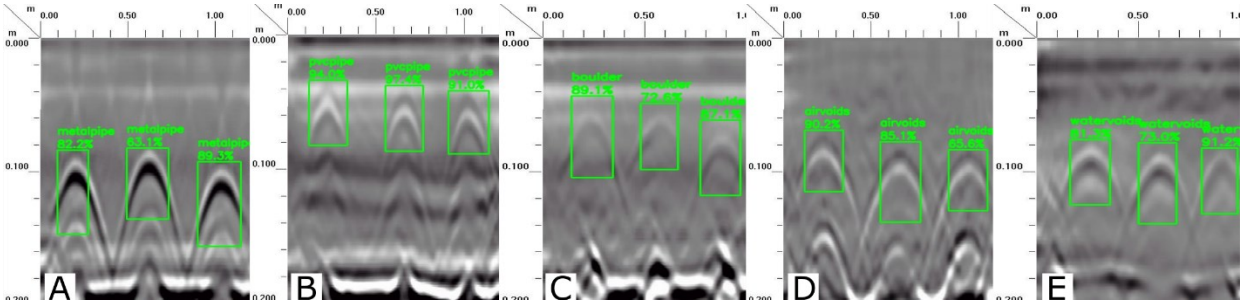

Figure 3-5: YOLO v3 results for metal pipes (A), PVC pipes (B), boulders (C), air voids (D) and water voids (E)

In order to determine the performance of the proposed method, precision, recall and F1 score were calculate and are presented in **Error! Reference source not found.**. The precision measures the

percentage of identified objects over all the objects present in the image, while recall indicates how many of the identified objects are correctly classified. In order asses the performance of the models, precision and recall were used to compute the F1 score.

TABLE 3-1: Precision, Recall and F1 score for YOLO v3 and R-CNN

Class	R-CNN			YOLO v3		
	Recall	Precision	F1 Score	Recall	Precision	F1 Score
Metal Pipe	1.00	0.42	0.59	1.00	0.86	0.91
PVC Pipe	1.00	0.43	0.59	0.74	0.79	0.88
Air Void	1.00	0.33	0.50	0.95	0.95	0.94
Water Void	1.00	0.33	0.50	0.78	0.81	0.74
Boulder	1.00	0.56	0.67	0.94	0.61	0.71
Average	1.00	0.41	**0.57**	0.88	0.80	**0.84**

Overall, R-CNN has better recall when classifying the features of the detected objects in the image i.e., when R-CNN correctly predicted an object location by assigning a bounding box around it, the class was correctly assigned in 100% of the cases. However, R-CNN was able to detect only one object per image, and, in some cases, the bounding boxes were assigned around background reflections, resulting in a precision of 41%. On the other hand, in 100% of the cases that YOLO v3 assigned a bounding box, it was in the correct location—i.e., the bounding box was just where hyperbolic reflections were present; however, the bounding box class was not always correctly assigned.

3.7. Summary and Conclusions

The use of ML to detect object features in GPR data is an important step to increase the accuracy of detection and reduce survey cost by decreasing the time spent on data analysis, when comparing to having extensive data analysis performed by person. This paper examined two deep learning algorithms, YOLO v3 and R-CNN, to select the one that has the best performance in detecting object features within GPR images. The test results showed that YOLO v3 outperformed R-CNN by presenting an F1 score of 84% versus 57%. R-CNN achieved 100% classification accuracy, i.e., the bounding boxes were correctly placed over hyperbolic reflections—however, R-CNN did not locate all hyperbolic reflections within the image achieving a detection accuracy of 41%. On the other hand, YOLO v3 achieved lower accuracy in object classification (88%) but was able to correctly identify 80% of the object reflections present within the images.

This research focused on the accurate detection and classification of objects in GPR images; however further studies are necessary to merge the classification accuracy achieved from R-CNN with the detection accuracy of YOLO v3. Moreover, adding object depth is recommended to increase detection parameters and improve the quality results. In addition, YOLO v3 should be applied in real time surveys to support the location of unexpected objects during construction, such as while drilling pilot bores in HDD.

4. Long-Term Performance Monitoring of Backfill Materials for Microtrenching in Cold Climates using Ground Penetrating Radar

4.1. Abstract

Ground penetrating radar (GPR) is a non-destructive tool that has been widely used in civil engineering projects to either support new construction (such as identifying potential conflicts in advance of utility installations) or to monitor existing installations. Microtrenching is a technique the offers remarkable advantages for fibre deployment, including less environmental disturbance and minimal surface restoration (compared to open-cut methods). MT installations involve the creation of a narrow trench, followed by laying a cable or conduit inside the trench, before backfilling and sealing the trench. The capacity of GPR to map the subsurface makes it an extremely valuable tool for monitoring the performance of microtrenching installations by flagging upward or downward displacement of the conduit inside the trench. This paper investigates conduit depth location of different backfill materials, during summer (survey conducted in August 2020), of a microtrenching installation performed in a cold region (Edmonton, Alberta, Canada) using visual inspection and GPR to assess any changes in conduit depth within the trench (along the installation path). The results indicate that GPR does give accurate readings, but additional measurements are needed during different seasons.

Keywords: Ground Penetrating Radar; Micro-trench; Fibre optics; Pavement backfill materials

4.2. Introduction

With advances in technology and changes in societal needs, the demand for real-time data transmission is increasing rapidly. The success of new applications—including remote medical treatment, autonomous vehicles, virtual and augmented reality, traffic operation sensors and municipal security systems—depends on the transmission of data in real time with high reliability and availability, as well as high security standards (Arnold et al. 2018; Singh and Rajan 2019). To address this need, there has been increased investment in expanding fiber to the x (FTTx – where x can be business, home or premises) networks installations to increase bandwidth capacity. Furthermore, widespread shifts observed in 2020/2021 towards working from home for many employees, due to the SARS-CoV-2 pandemic, has increased the need for reliable internet access to a higher number of homes. With the increasing demand for FTTx, the challenge of deploying

fibre installations with minimal cost and disturbance to society and the environment becomes even more important.

Fibre installations are done in the subsurface and traditional installations depend on open-cut installations, which generally cause traffic disruptions, surface scarring, and economic and environmental impact on surrounding business and residents (Atalah et al. 2012). To address the challenges associated with fibre deployment, new technologies, such as micro-trenching, have been introduced. Such technologies have the advantage of minimal disturbance to the community and environment during construction, as well as lower cost and construction times compared to traditional construction methods (Hashemian et al. 2017). The long-term performance of MT depends on the prevention of conduit movement inside the trench, as well as maintaining the integrity of the pavement surrounding the trench. Both of these considerations depend directly on the backfill material, the performance of which can vary significantly depending on weather conditions (Hasanuzzaman 2016). For example, Hashemian et al. observed that for installation in cold climates, backfill materials must be selected to withstand potential frost heaving (caused by frost penetration and high water tables) (2017). Once the proper backfill materials have been selected and the fibre has been deployed, long-term monitoring of the installation is necessary to confirm that the MT design withstands the environmental conditions.

GPR has been widely used as a non-destructive tool for subsurface mapping, including to investigate the performance of new and existing underground utilities. Multiple articles have been published related to the capability of GPR to locate underground utilities, mainly to support underground excavation by reducing the uncertainty associated with excavation and thus avoiding damage of existing utilities (Dave and Agrawal 2018; Metwaly 2015; Porsani et al. 2012). However, despite the many applications of GPR for underground mapping, little information has been published regarding the use of GPR for long-term monitoring of MT installations in cold climates. In previously published research, Hasanuzzaman (2016) monitored the performance of MT under traffic loads and in cold weather conditions, with results showing significant cable displacement inside the trench and premature failure of backfill materials. Similarly, Hashemian et al. (2017) monitored a pilot MT installation using GPR over three years. In this work, GPR and visual inspections showed vertical displacement of the conduit in the trench and failure of backfill material over time.

4.3. Objectives and Scope

The main objective of this research is to investigate the applicability of GPR in determining the conduit depth within the MT, and to assess the service life of different backfill materials for MT in cold climates. To achieve this, several GPR measurements were conducted for a pilot MT installation, to localize and determine conduit depth and compare with previous surveys to determine conduit movement in the MT. In addition to measuring horizontal cable displacement, GPR was also used to determine asphalt layer depth in the MT.

4.4. Methodology

4.4.1. Microtrenching Installations

To investigate conduit location at a MT installation performed in cold climate under different traffic conditions, a GPR survey was conducted in August 2020 at a pilot MT installation located in the private parking lot of a corporate-owned operational building located in Edmonton, AB, as shown in Figure 4-1. Traffic loading in the installation area was due to the movement of cars and garbage trucks. At this location, MT installations using two different technologies (VIF and SMCI) and different backfill materials were installed in October 2013, July 2014, July 2016, and September 2016. All MT fibre installations involved marking the installation path, followed by cutting and cleaning the trench. Then, the cable or conduit was laid, followed by the application of backfill material. A description of the installation layout and backfill materials, as well as a discussion of conduit location, as determined using GPR, is included in the following sections.

Figure 4-1: Microtrench installation layouts

4.4.2. Backfill Materials

The first fibre installation was done in October 2013, with three vertical inlaid fibre (VIF) installations completed. The trench dimensions for VIF were 1.5 cm wide and 22.8 cm deep, with a backfill design consisted of a layer of playground sand, followed by Perma-Patch cold mix asphalt (CMA) (Figure 4-2). All three VIF installations had the same backfill design but varied in size and traffic loading (due to cars and garbage trucks). The installations were as follows: a 30-m linear installation located in the path of traffic (VIF-A); a 30-m linear installation located in the path of traffic (VIF-B); and a 55-m loop located directly in the path of traffic (VIF-C). In the third installation, a vertical deflecting conduit (VDC) was used, with a wire tracer included in one channel. The wire tracer, which is a complete reflector, is extremely helpful for GPR detection of the VDC (and thus determination of fibre depth) because it reflects all the energy received from the GPR, while the surrounding material absorbs part of the energy.

In June 2014, an MT installation in an area without traffic loading (SCMI-A), as well as a 72-m loop directly in the path of traffic (SCMI-B) were performed. Both installations were done using surface micro cable inlay (SMCI) in a trench that was 0.9 cm wide and 7.6 cm deep (Figure 4-2). The SMCI installation consisted of a fiber optic cable, followed by a foam spacer and rubber strip covered with playground sand and hot bitumen sealant as backfill.

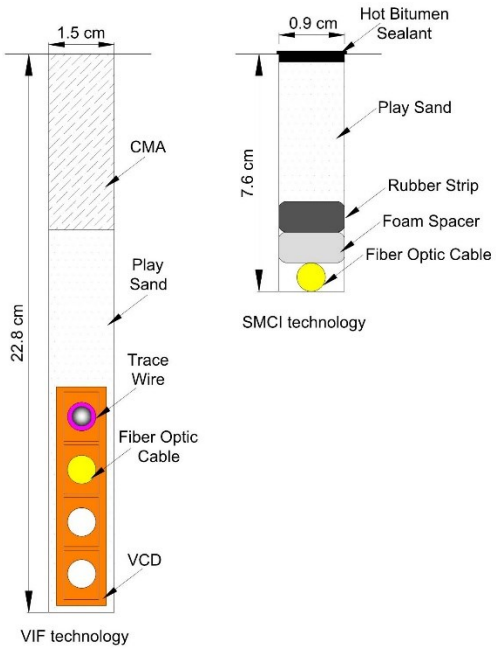

Figure 4-2: VIF and SMCI installations layouts

For both the VIF and SCMI MT installations, the specifications and performance of the backfill materials used—e.g., uniformly graded playground sand (with small particle size), hot bitumen sealant, and Perma-Patch CMA)—were confirmed through laboratory testing. Details related to the testing procedures and material characteristics have been reported previously by Hashemian, Rezaei, and Bayat (2017).

4.4.3. Ground Penetrating Radar

GPR involves sending an electromagnetic (EM) signal from a transmitting antenna. The EM signal travels through the ground and is reflected when it hits an object or subsurface layer that has different electrical properties from the surrounding medium (Daniels 2000). The higher the difference in electrical properties between the feature and the surrounding material, the stronger and clearer is the observed signal (Geophysical Survey Systems, Inc 2016). This is the reason that

VIF technology, which includes a wire tracer, results in clearer GPR determinations of conduit location compared to SMCI.

Electromagnetic waves travel at specific velocities that are determined primarily by the permittivity (i.e., the ability of a material to store and release EM energy) of the material (Daniels 2000). For this reason, the capability of GPR for investigation of MT performance is influenced directly by accurate prediction of the dielectric constant (also known as relative permittivity) of the material in which the EM wave travels (Leng and Al-Qadi 2014). This is related to velocity as shown in Equation (1),

$$v = \frac{c}{\varepsilon_r} \quad (1)$$

where v is the wave propagation speed, c is the speed of light in free space (3×10^8 m/s) and ε_r is the relative permittivity.

By rearranging Equation 1 and replacing the velocity with the distance travelled by the electromagnetic wave, d, divided by time, t, Equation 2 can be derived.

$$\varepsilon_r = \frac{c \times t}{d} \quad (2)$$

In this case, the EM velocity (ns) within the material used to fill the MT is determined using GPR measurements. The depth of the conduit (d) was determined by opening a small area of the trench to expose the conduit (Figure 4-3). Using these two measured quantities, the dielectric constant of the material was determined. As seen from Equation 2, a slight increase in the dielectric constant leads to an error in the GPR reading, indicating a shallower conduit. For the purpose of this research, all surveys were conducted in similar conditions (i.e., no change in moisture content) and the conduit depth was confirmed for each section. This resulted in a determination of a dielectric constant of 6.9 for the backfill materials used in this work. The lack of variation in the value of the dielectric constant determined for the different MT installations can be explained by the similarity of the properties of the various backfill materials.

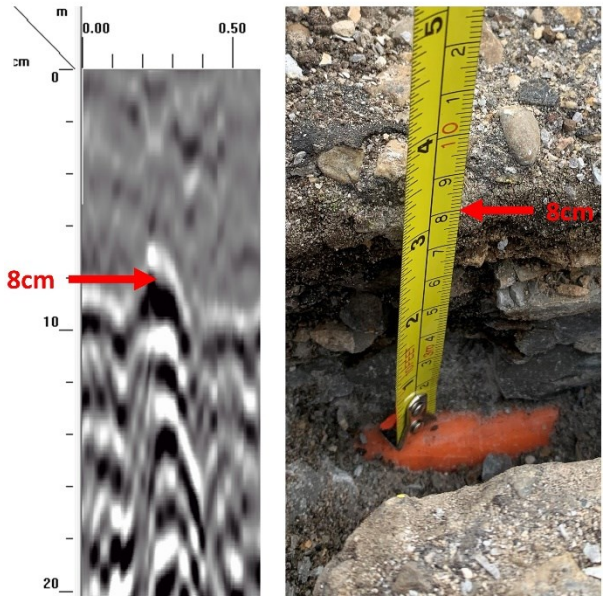

Figure 4-3: Determination of dielectric value based on a measurement of conduit depth in an open trench

4.4.4. GPR Data Acquisition and Processing

GPR data acquisition was done using a GSSI-SIR 4000 GPR (Geophysical Survey Systems, Inc.) coupled with a palm antenna of 2000 MHz (GSSI, Model 62000). A high frequency antenna was chosen because it gives high resolution at shallower depths, with a low penetration depth. This fits the requirements for the investigation of MT installations, which are typically shallower than 30 cm. Additional data collection parameters are specified in TABLE 4-1.

TABLE 4-1: Parameters used for GPR data acquisition

GPR system	SIR-4000
Antenna frequency	2000 MHz
Transmission rate	2000 MHz
Collection mode	Distance
Samples/Scan	512
Dielectric	6.9
Filters	400–5000 MHz
Gain	Automatic

Horizontal calibration of the GPR unit was done using a measuring tape. Vertical calibration was done by opening a small section of each trench. In this way, it was possible to precisely determine

the conduit depth (as in Equation 1) and thus determine the dielectric constant. Opening the trench to calibrate the depth measurements was found to be the best option to ensure a high level of confidence in determining conduit depth. This is because each of the different materials present in the trench has a different dielectric constant, making it difficult to determine a single dielectric value to use as an input for interpretation of the GPR data. Furthermore, knowledge of the material type is not enough to characterize the dielectric constant, since compaction also should be considered. Compaction reduces the quantity of air (which has a low dielectric constant) in the backfill material, thus increasing the volumetric proportion of components with higher dielectric constants (e.g., sand and CMA), which results in higher dielectric values for compacted materials (Saarenketo 1997).

To precisely determine the conduit location and thickness of the asphalt layer, data collection was performed in two directions, by conducting surveys parallel and perpendicular to the trench (Figure 4-4). The parallel survey results in an image with a continuous line indicating the conduit depth along the installation path. In contrast, perpendicular surveys images show a hyperbolic reflection, corresponding to the local depth of the conduit, and therefore this data needs to be interpolated between two perpendicular measurements. Perpendicular surveys also show a first-layer reflection which corresponds to the asphalt depth. Ideally, perpendicular (depth) measurements and parallel measurements should be performed to ensure the accuracy of the survey; however, for the SMCI sections, the parallel survey did not give a clear reflection of conduit location. In contrast, VIF, which includes a trace wire, showed clear parallel reflections, as depicted in Figure 4-4.

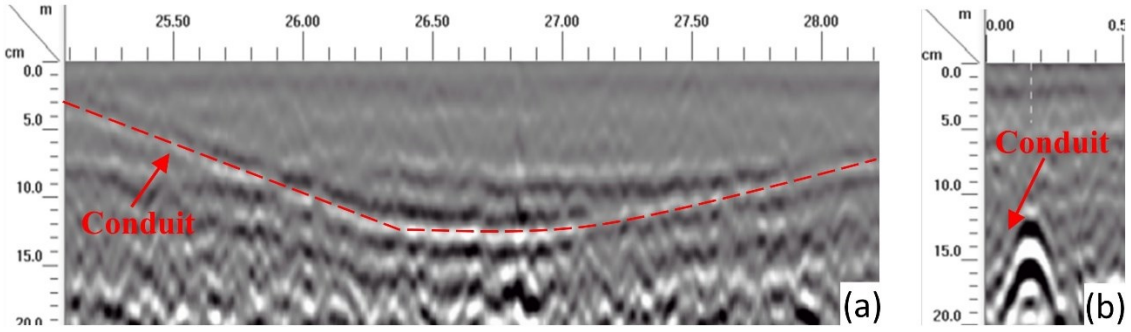

Figure 4-4: GPR image showing conduit reflection during (a) parallel and (b) perpendicular surveys

After performing data collection, GPR images were filtered to reduce noise and the effect of equipment instability, such as signal drift, giving data that were easier to interpret (Szymczyk and Szymczyk 2013). The most commonly used filters for GPR data are time zero correction, background removal, gain, and high- and low-pass filters. In this study, background removal, which is used to remove horizontal bands of noise, was only applied to data collected in the perpendicular survey. If background removal were to be applied to data from the parallel survey, it could remove the horizontal reflection due to the wire, i.e., the target reflection. Low- and high-pass filters were used to remove noise by attenuating signal frequencies below (for high-pass filters) and above (for low-pass filters) a selected cutoff frequency (Hinterleitner et al. 2009).

4.5. Field Monitoring Results

4.5.1.1. VIF Installation Monitoring Results

GPR data was acquired during monitoring inspections (conducted on November 8, 2013; May 12, 2014; July 30, 2014; and May 4, 2015) of the VIF pilot installations on the 30-m linear installations with and without traffic loading and the 55-m loop with traffic loading (Vaseli 2015). In addition, Rios (2018) reported the results of a GPR survey conducted in September 2018 for the 55-m loop located in the direct path of traffic (Figure 1, red loop). Another GPR survey of all MT installations was performed on August 13, 2020. These results were compared to previous measurements.

4.5.1.2. VIF Installation with no Traffic Loading

Historical GPR data for the 30-m VIF installation with no traffic loading, was available from a monitoring survey conducted six months after installation (a time period which included one winter). After 18 months (including two winters) the conduit was almost horizontal, with a maximum upward displacement of 8.9 cm compared to the original location (Hashemian et al. 2017). After almost seven years of installation (a total of 81 months, including seven winters), the maximum upward displacement was 10.3 cm. These results indicate that the most significant displacement of the conduit, including upward and downward displacements, occurred in the first two years after installation (Figure 4-5a). This can be confirmed by comparing the conduit depth in August 2020 and May 2015: at two locations, a maximum upward displacement of 3.5 cm was observed, while along the remaining installation path, the conduit maintained its previous depth.

A visual observation of the MT installation path showed the presence of vegetation, which could facilitate the entry of water into the trench (Figure 4-5b).

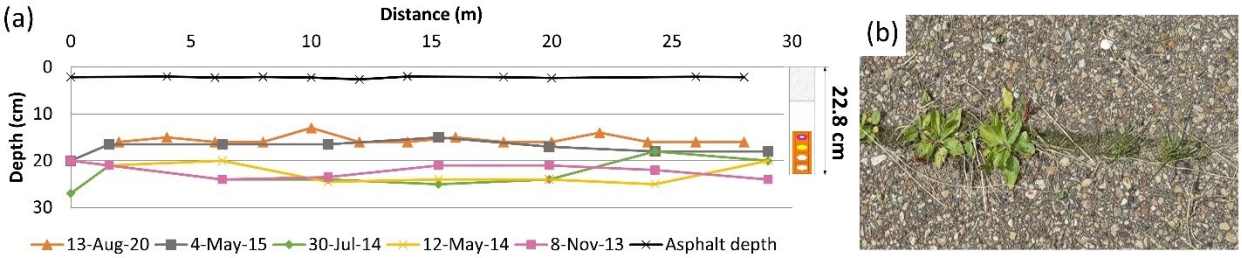

Figure 4-5: (a) Conduit displacement within trench based on GPR monitoring of the 30 m linear VIF installation without traffic loading, and (b) presence of vegetation in the MT (~seven years after installation)

4.5.1.3. VIF Installation with Traffic Loading

GPR monitoring of the 30 m linear VIF installation in the area of the parking lot with traffic loading was conducted after six months of installation, in May 2014. At this time, the conduit showed a maximum downward displacement of 6 cm (located within the 5 last meters of the installation) and an upward displacement of 2 cm (at the starting point of the installation). After nine months (July 2014), the conduit showed an upward displacement of 12 cm relative to the initial position (within the last 5 m of the installation) and a maximum downward displacement of 4 cm. After 18 months (May 2015), including two winters, the displacement of the last 5 m of conduit, which showed the maximum displacement according to the previous measurement, was reduced to 2 cm (relative to the original conduit depth). The conduit showed a maximum upward displacement of 6 cm in the same survey. The last survey, which was performed in 2020, indicated that the greatest conduit displacement occurred in the last 7 m of the installation. This is similar to observations in previous surveys, which showed that the loose end of the conduit resulted in freedom of movement near the end of the installation path, with an upward displacement of 15.8 cm observed. In contrast, within the remaining 23 m of the installation, no major displacements were observed (compared to 2015 measurements)—Figure 4-6.

In addition to GPR results, visual inspections indicated that the CMA has low adhesion to the sides of the microtrench. According to Hashemian et al. (2017), one of the reason for the poor adhesion is the presence of water during the process of cutting the microtrench, which made the trench walls muddy and decreased adhesion between the CMA (used as backfill material) and the existing

HMA layer during installation. Furthermore, in 2020, visual inspection indicated that the pavement surrounding the MT showed severe distresses, such as alligator cracks, in the direct path of traffic load (garbage truck path). These distresses caused differential settlement of the MT which occurred because of the infiltration of water and escape of the playground sand used as backfill (according to Hashemian et al. (2017)).

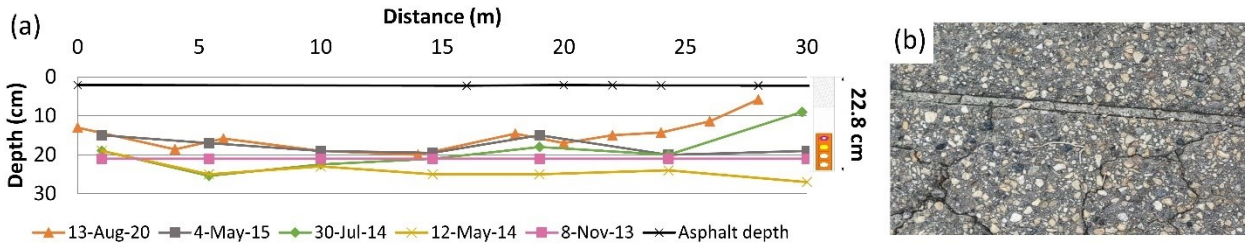

Figure 4-6: (a) Conduit displacement within trench based on GPR monitoring of the 30m VIF installation with traffic load, and (b) alligator cracking near path of VIF MT installation (seven years after installation)

4.5.1.4. 55 m VIF Loop with Traffic Loading

Historical GPR data for the 55-m VIF loop located directly in the path of traffic six months after installation showed a conduit displacement of 5.9 cm downwards (the maximum observed downward displacement) and 14.3 cm upwards—for context, these movements occurred in a trench 22.8 cm deep (Hashemian et al. 2017). In addition, after nine months the conduit showed only upward displacement, with a maximum displacement of 14.3 cm relative to the initial position (Figure 4-7a). After that time, only upward displacements were observed, culminating in appearance of the conduit at the surface in 2020 (Figure 4-7b). The portion of the trench where the conduit appeared at the surface was located near some garbage bins and corresponded to the area of the parking lot in the traffic path of garbage truck and smaller vehicles. Visual inspections of the pavement done in previous years at this location (Rios 2018) indicated alligator cracking and permanent pavement deformation, which could be due to excessive water in the granular base layer. It is reasonable to attribute the poor performance of the MT fibre installation in this area to the deterioration in pavement conditions, rather than the MT construction methods and backfilling materials.

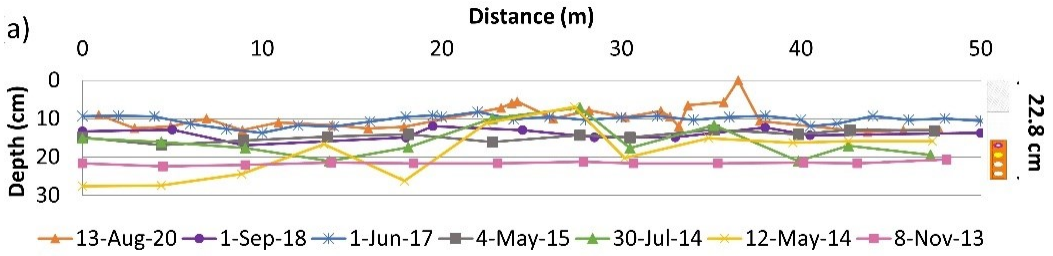

Figure 4-7: (a) Conduit displacement within trench based on GPR monitoring of the 55 m VIF loop installation with traffic loading

4.5.2. SMCI Installation Monitoring Results

For the SMCI technology, data from three previous GPR surveys was available, one conducted on July 30, 2014, one on May 4, 2015 (Vaseli 2015), and another survey in 2018 (Rios 2018). The results of the 2020 survey were compared with all previous measurements.

4.5.2.1. 30 m SMCI Installation with no Traffic Loading

The first survey on the 30-m SMCI installation (no traffic loading) was performed one month after installation of the conduit and showed an almost horizontal distribution of the conduit (same conduit depth along MT installation) around the original installation depth of 7.6 cm a). Ten months after installation, the conduit showed a maximum upward displacement of 2.5 cm from the initial installation depth. GPR results from the survey conducted in 2020 showed a maximum downward displacement of 1 cm (compared to the initial installation depth), which was observed in the first 4 m of the installation, and a maximum upward displacement of 2.5 cm. This indicates that there were no significant changes in depth (compared to the GPR monitoring conducted in 2015). Visual inspection confirmed that six years after the installation, the MT is in good condition and the sealant is intact (Figure 4-8b).

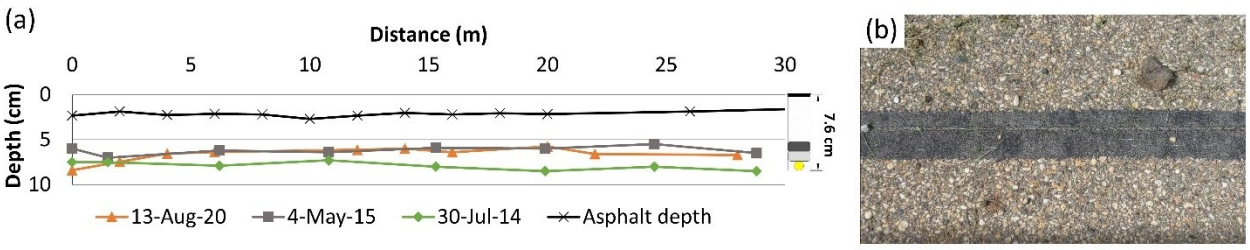

Figure 4-8: (a) Conduit displacement within trench (based on GPR monitoring) of a 30 m SMCI installation without traffic load. (b) Current condition of MT installation, as observed from the surface

4.5.2.2. 72 m SMCI Installation with Traffic Loading

A GPR survey performed in the same year of the 72-m SMCI installation with traffic loading indicated that the conduit was located at a shallower depth in the trench compared to the design depth (7.6 cm) for the last 20 m of the installation. This could be due to a variation in the depth of the trench or backfill material during trench construction (**Error! Reference source not found.**a). Since the construction and the survey were done only two months apart, at a time of year without considerable temperature changes, the survey can be considered to give the as-built conduit depth. The tendency of cable displacement towards the surface over these last 20 m was also observed in the 2020 survey, with a maximum upward and downward displacement of the conduit in that area of 3.3 cm and 1.5 cm, respectively, compared to 2014 survey results. Visual inspection indicated that the MT was in good condition, with the sealant intact (Figure 4-9).

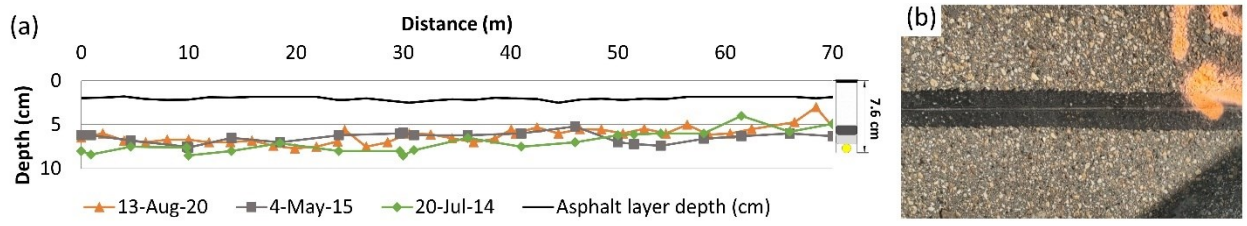

Figure 4-9: (a) Conduit displacement within trench based on GPR monitoring of a 72-m SMCI installation with traffic loading. (b) Portion of SMCI MT installation showing good overall condition

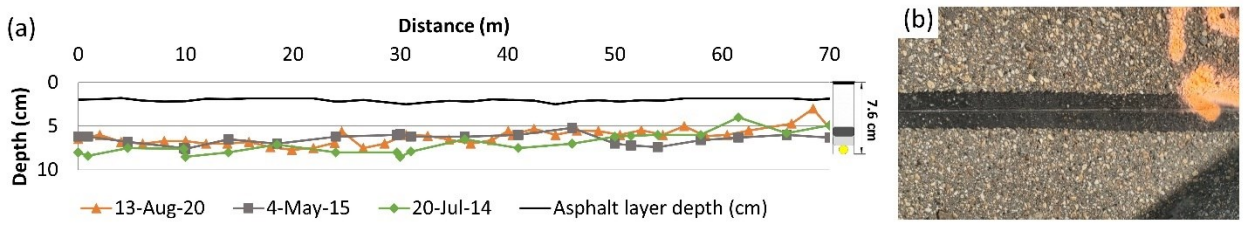

Figure 4-9: (a) Conduit displacement within trench based on GPR monitoring of a 72-m SMCI installation with traffic loading. (b) Portion of SMCI MT installation showing good overall condition

4.6. Summary and Conclusions

This study used GPR to evaluate the long-term conduit displacement in MT installations in cold regions. The MT installations monitored had different layouts (with and without traffic loading) and different backfill materials. Based on the results of GPR monitoring, the following conclusions were reached:

1. GPR is a useful tool for determining conduit depth within the MT, provided that the dielectric of the material can be accurately determined. VIF conduit, which includes a trace wire, gives clearer GPR readings and therefore more accurate results.
2. GPR showed good results to track the movements
3. All VIF installations showed upward displacement of the conduit. The straight installation (without traffic loading) showed the lowest maximum vertical displacement (10.3 cm). The straight installation with traffic loading resulted in the highest vertical displacement, a displacement of 15.8 cm observed at the end the MT installation, possibly due to a loose conduit end. The maximum vertical displacement in the loop installation occurred in an area of higher traffic.
4. The SMCI installation with no traffic loading resulted in a maximum downward displacement of 1 cm and maximum upward displacement of 2.5 cm (the initial installation depth was 7.6 cm). The SMCI installation with traffic loading resulted in a maximum downward displacement of 1.5 cm and maximum upward displacement of 3.3 cm. Similar to the results observed for the VIF installation, the SMCI installation with traffic loading showed a maximum upward displacement at the end of the MT installation, which again could be due to a loose conduit end.

5. Summary and Conclusions

5.1. Summary

Developing sustainable and reliable infrastructure is vital to equip urban areas with infrastructure that is adequate to serve growing populations. With the increased need for new infrastructure and rehabilitation of sewer, water, gas, telecommunication and other lines, underground construction has increasingly been used to meet these demands. The use of technologies such as GPR have been widely used to map the subsurface and support underground infrastructure installations—however, the interpretation of GPR images can still improve in efficiency with the use of ML techniques.

The focus of this study was to assess ML capabilities in the automation of underground object detection in GPR images. For this purpose, a comprehensive literature review to understand previously applied ML methodologies in the automatic detection of objects in GPR images was performed. The use of two ML algorithms—YOLO v3 and R-CNN— used in laboratory collected images was proposed to achieve fast and accurate detections.

A secondary objective was to continue a previous study that employed GPR technology for the long-term performance evaluation of MT backfill materials for fiber optics installation. To achieve this, GPR surveys of a MT pilot installation were conducted and compared to previous studies performed in the same area to detect conduit movement.

5.2. Conclusions

Two ML algorithms were tested for the automated interpretation of GPR images in order to compare performance and determine and most accurate algorithm for automatic object detection. In addition, GPR was used in the long-term performance assessment of MT backfill materials. The conclusions obtained are summarized as follows:

1. YOLO v3 outperformed R-CNN and achieved an 84% (versus 57%) F1 score, which confirmed the suitability of the model for the detection of underground object features within GPR images.
2. R-CNN achieved the best recall (100% versus 88%) and was able to correctly classify all accurately detected objects. However, R-CNN was just able to detect 41% of the hyperbolic reflections present within an image.

3. YOLO v3 was able to identify 80% of all hyperbolic reflections present in the images and achieved good overall accuracy by correctly assigning classes to the identified reflections.
4. GPR gave accurate results of conduit location after precisely determining the dielectric permittivity of each backfill material.
5. GPR surveys are easier to interpretate when complete reflector objects such as a wire tracer are present.

5.3. Future Research

Future research is recommended to increase the algorithm F1 score (overall accuracy which includes object detection and classification accuracies) and to assess the generalization capabilities of the tested algorithms for automated processing of GPR images in scenarios different than the ones tested in this research. It is recommended that the existing database of GPR images be expanded by performing surveys with different equipment in various locations for a variety of underground objects and subsurface materials (i.e., different types of soils). These variations might result in different noise levels in the training images, which can impact detection accuracy. In addition, the creation of an online database of labeled GPR images ready for the application of different ML algorithms would speed up further developments in the automation of object detection based on GPR images.

The newly developed ML methodology should be applied and tested in real time during a GPR survey of the MT installations. Additional GPR surveys of the pilot MT installations are recommended to compare the performance of the installation in different temperature conditions (seasons).

Bibliography

Al-Jawfi, R. (2009). "Handwriting Arabic character recognition LeNet using neural network." *The International Arab Journal Information Technology*, 6(3), 304–309.

Allouche, E. N., Ariaratnam, S. T., and Lueke, J. S. (2000). "Horizontal Directional Drilling: Profile of an Emerging Industry." *Journal of Construction Engineering and Management*, American Society of Civil Engineers, 126(1), 68–76.

Al-Nuaimy, W., Huang, Y., Eriksen, A., and Nguyen, V. T. (2001). "Automatic detection of hyperbolic signatures in ground-penetrating radar data." *Subsurface and Surface Sensing Technologies and Applications III*, International Society for Optics and Photonics, 327–335.

Al-Nuaimy, W., Huang, Y., Nakhkash, M., Fang, M. T. C., Nguyen, V. T., and Eriksen, A. (2000). "Automatic detection of buried utilities and solid objects with GPR using neural networks and pattern recognition." *Journal of Applied Geophysics*, 43, 157–165.

Alzubi, J., Nayyar, A., and Kumar, A. (2018). "Machine Learning from Theory to Algorithms: An Overview." *Journal of Physics: Conference Series*, IOP Publishing, 1142, 012012.

Arcand, L., Eng, P., and Osman, H. (2006). "Utilization of Subsurface Utility Engineering to improve the effectiveness of Utility Relocation and Coordination efforts on Highway Projects in Ontario." *Proceedings of Annual Conference of the Transportation Association of Canada, Charlottetown*, 17–20.

Ardekani, S. (2006). "Automatic and fast detection of buried utilities positions and estimation of soil permittivity using GPR." *11th International Conference on Ground Penetrating Radar*.

Arnold, R., Kroon, P., Tas, S., and Tenbrock, S. (2018). *The socio-economic impact of FTTH*. WIK-Consult, Bad Honnef, Germany.

ASCE. (2002). "Standard guidelines for the collection and depiction of existing subsurface utility data." American Society of Civil Engineers.

Atalah, A., Chang-Jin, C., and Osburn, K. (2012). "Comparison Study of Installing Fiber Optic Cable in University Campuses Using Trenchless Techniques Relative to Open Cut." American Society of Civil Engineers, 1–17.

Avan, Erfiani, and Sartono, B. (2017). "Comparison of Backpropagation and Resilient Backpropagation Algorithms in Non-Invasive Blood Glucose Measuring Device." *International Journal of Scientific & Engineering Research*, 8(8), 5.

Basak, J., and Das, A. (2003). "Hough transform network: a class of networks for identifying parametric structures." *Neurocomputing*, 51, 125–145.

Benjdira, B., Khursheed, T., Koubaa, A., Ammar, A., and Ouni, K. (2019). "Car Detection using Unmanned Aerial Vehicles: Comparison between Faster R-CNN and YOLOv3." *Proceedings of the 1st International Conference on Unmanned Vehicle Systems (UVS)*, 1–6.

Besaw, L. E., and Stimac, P. J. (2015). "Deep convolutional neural networks for classifying GPR B-scans." *Proceedings of SPIE 9454*, 945413, International Society for Optics and Photonics.

Bianchini Ciampoli, L., Tosti, F., Economou, N., and Benedetto, F. (2019). "Signal Processing of GPR Data for Road Surveys." *Geosciences*, Multidisciplinary Digital Publishing Institute, 9(2), 96.

Birkenfeld, S. (2010). "Automatic detection of reflexion hyperbolas in GPR data with neural networks." *2010 World Automation Congress*, Kobe, Japan, 1–6.

Buslaev, A., Parinov, A., and Khvedchenya, E. (2018). "Albumentations: fast and flexible image augmentations." *Information*, 11(2), 125.

Capineri, L., Grande, P., and Temple, J. a. G. (1998). "Advanced image-processing technique for real-time interpretation of ground-penetrating radar images." *International Journal of Imaging Systems and Technology*, 9(1), 51–59.

Cazzaniga, N., Carrion, D., Migliaccio, F., and Barzaghi, R. (2013). "A shared database of underground utility lines for 3D mapping and GIS applications." 105–108.

Daniels, J. J. (2000). "Ground penetrating radar fundamentals." *Prepared as an appendix to a Report to the US EPA, Region V*, 1–21.

Dave, K., and Agrawal, S. (2018). “Non-destructive Technology for Underground Utility Mapping: A Case Study.” *Proceedings of China-Europe Conference on Geotechnical Engineering*, Springer Series in Geomechanics and Geoengineering, W. Wu and H.-S. Yu, eds., Springer International Publishing, Cham, 1136–1139.

Deng, J., Dong, W., Socher, R., Li, L., Li, K., and Fei-fei, L. (2009). “Imagenet: A large-scale hierarchical image database.” *2009 IEEE Conference on Computer Vision and Pattern Recognition*, 248–255.

Dérobert, X., and Pajewski, L. (2018). “TU1208 Open Database of Radargrams: The Dataset of the IFSTTAR Geophysical Test Site.” *Remote Sensing*, Multidisciplinary Digital Publishing Institute, 10(4), 530.

Dhillon, A., and Verma, G. K. (2020). “Convolutional neural network: a review of models, methodologies and applications to object detection.” *Progress in Artificial Intelligence*, 9(2), 85–112.

Dou, Q., Wei, L., Magee, D., and Cohn, A. (2017). “Real-Time Hyperbolae Recognition and Fitting in GPR Data.” *IEEE Transactions on Geoscience and Remote Sensing*, Institute of Electrical and Electronics Engineers, 55(1), 51–62.

Du, J. (2018). “Understanding of Object Detection Based on CNN Family and YOLO.” *Journal of Physics: Conference Series*, IOP Publishing, 1004, 012029.

Duda, R. O., and Hart, P. E. (1972). “Use of the Hough transformation to detect lines and curves in pictures.” *Communications of the ACM*, ACM New York, NY, USA, 15(1), 11–15.

EM Software and System. (2005). *FEKO Suite 5.1*.

Ertam, F., and Aydın, G. (2017). “Data classification with deep learning using Tensorflow.” *2017 International Conference on Computer Science and Engineering (UBMK)*, 755–758.

Everingham, M., Van Gool, L., Williams, C. K. I., Winn, J., and Zisserman, A. (2010). “The Pascal Visual Object Classes (VOC) Challenge.” *International Journal of Computer Vision*, 88(2), 303–338.

Geophysical Survey Systems, Inc. (2016). “SIR 4000 Manual.” Nashua, NH, US.

Giannopoulos, A. (2005). *GprMax: A ground penetrating radar simulation tool*. Univ. of Edinburgh Edinburgh, UK.

Girshick, R. (2015). “Fast R-CNN.” *Proceedings of the IEEE International Conference on Computer Vision*, 1440–1448.

Girshick, R., Donahue, J., Darrell, T., and Malik, J. (2014). “Rich feature hierarchies for accurate object detection and semantic segmentation.” *arXiv:1311.2524 [cs]*.

Golovko, M. (2007). “The Evaluation of Performances of Automatic Method for the Object Detection in GPR Images.” *2007 5th International Symposium on Image and Signal Processing and Analysis*, 476–481.

Gong, Z., and Zhang, H. (2020). “Research on GPR image recognition based on deep learning.” *MATEC Web of Conferences*, EDP Sciences, 309(03027).

GSSI. (2016). “Utility Locating Handbook.” 37.

Hall, K. T., Correa, C. E., Carpenter, S. H., and Elliott, R. P. (2002). “Guidelines for evaluation of highway pavements for rehabilitation.” *Pavement Evaluation Conference*, Roanoke, Virginia, USA.

Hasanuzzaman, M. (2016). “An Investigation on Micro-Trenching Technology for FTTH Deployment.” Master of Science, University of Alberta, Edmonton, AB.

Hashemi, M. (2019). “Enlarging smaller images before inputting into convolutional neural network: zero-padding vs. interpolation.” *Journal of Big Data*, 6(1), 98.

Hashemian, L., Rezaei, M., and Bayat, A. (2017). “Field and laboratory investigations on pavement backfilling material for micro-trenching in cold regions.” *International Journal of Pavement Research and Technology*, 10(4), 333–342.

Hinterleitner, A., Seren, S., Löcker, K., Neubauer, W., and Bayirli, E. (2009). “Data Processing and Image Enhancement of GPR Surveys of Roman Villas in Austria.” *ArcheoSciences. Revue d’archéométrie*, Presses universitaires de Rennes, (33 (suppl.)), 299–302.

Huang, Z., Li, F., Luan, X., and Cai, Z. (2020). “A Weakly Supervised Method for Mud Detection in Ores Based on Deep Active Learning.” *Mathematical Problems in Engineering*, Hindawi, 2020, e3510313.

Jakkula, V. (2006). "Tutorial on support vector machine (SVM)." *School of EECS, Washington State University*, 37.

Kaur, P., Dana, K. J., Romero, F. A., and Gucunski, N. (2016). "Automated GPR Rebar Analysis for Robotic Bridge Deck Evaluation." *IEEE Transactions on Cybernetics*, 46(10), 2265–2276.

Khan, A., Qureshi, A. S., Wahab, N., Hussain, M., and Hamza, M. Y. (2016). "A Recent Survey on the Applications of Genetic Programming in Image Processing." *arXiv*, abs/1901.07387.

Kim, N., Kim, K., An, Y.-K., Lee, H.-J., and Lee, J. J. (2018). "Deep learning-based underground object detection for urban road pavement." *International Journal of Pavement Engineering*, 1–13.

Kobashigawa, J. S., Youn, H., Iskander, M. F., and Yun, Z. (2011). "Classification of Buried Targets Using Ground Penetrating Radar: Comparison Between Genetic Programming and Neural Networks." *IEEE Antennas and Wireless Propagation Letters*, 10, 971–974.

Köppen, M., Soria-Frisch, A., and Vicente-García, R. (2001). "NeuroHough: A Neural Network for Computing the Hough Transform." *Artificial Neural Nets and Genetic Algorithms*, V. Kůrková, R. Neruda, M. Kárný, and N. C. Steele, eds., Springer Vienna, Vienna, 197–200.

Koza, J. R., Bennett, F. H., Andre, D., and Keane, M. A. (1999). *Genetic Programming III: Darwinian Invention and Problem Solving*. Morgan Kaufmann, San Francisco.

Krizhevsky, A., Sutskever, I., and Hinton, G. E. (2012). "ImageNet Classification with Deep Convolutional Neural Networks." *Advances in Neural Information Processing Systems*, (F. Pereira, C. J. C. Burges, L. Bottou, and K. Q. Weinberger, eds.), 25, 1097–1105.

LeCun, Y., Boser, B. E., Denker, J. S., Henderson, D., Howard, R. E., Hubbard, W. E., and Jackel, L. D. (1990). "Handwritten digit recognition with a back-propagation network." *Advances in neural information processing systems*, 396–404.

Lecun, Y., Bottou, L., Bengio, Y., and Haffner, P. (1998). "Gradient-based learning applied to document recognition." *Proceedings of the IEEE*, 86(11), 2278–2324.

Leng, Z., and Al-Qadi, I. L. (2014). "An innovative method for measuring pavement dielectric constant using the extended CMP method with two air-coupled GPR systems." *NDT & E International*, 66, 90–98.

Lin, T.-Y., Maire, M., Belongie, S., Hays, J., Perona, P., Ramanan, D., Dollár, P., and Zitnick, C. L. (2014). "Microsoft COCO: Common Objects in Context." *Computer Vision – ECCV 2014*, D. Fleet, T. Pajdla, B. Schiele, and T. Tuytelaars, eds., Springer International Publishing, Cham, 740–755.

Liu, G., Jia, Y., Liu, H., Qiu, H., Qiu, D., and Shan, H. (2002). "A Case Study To Detect the Leakage of Underground Pressureless Cement Sewage Water Pipe Using GPR, Electrical, and Chemical Data." *Environmental Science & Technology*, American Chemical Society, 36(5), 1077–1085.

Maas, C., and Schmalzl, J. (2013). "Using pattern recognition to automatically localize reflection hyperbolas in data from ground penetrating radar." *Computers & Geosciences*, 58, 116–125.

Macukow, B. (2016). "Neural Networks – State of Art, Brief History, Basic Models and Architecture." *Computer Information Systems and Industrial Management*, Lecture Notes in Computer Science, K. Saeed and W. Homenda, eds., Springer International Publishing, Cham, 3–14.

Manacorda, G., Miniati, M., Simi, A., Guidi, R., Lelli, S., Vacca, D., Dei, D., Mecatti, D., Scott, H. F., Morey, M., Hamers, M., and Schauerte, T. (2014). "A bore-head GPR for horizontal directional drilling (HDD) equipment." *Proceedings of the 15th International Conference on Ground Penetrating Radar*, 745–750.

McCulloch, W. S., and Pitts, W. (1943). "A logical calculus of the ideas immanent in nervous activity." *The bulletin of mathematical biophysics*, 5(4), 115–133.

Metwaly, M. (2015). "Application of GPR technique for subsurface utility mapping: A case study from urban area of Holy Mecca, Saudi Arabia." *Measurement*, 60, 139–145.

Mita, T., Kaneko, T., and Hori, O. (2005). "Joint Haar-like features for face detection." *Tenth IEEE International Conference on Computer Vision (ICCV'05)*, 1619–1626.

Moganti, P. Y. (2016). "Safety risk investigation of Horizontal Directional Drilling projects."

Molyneaux, T. C. K., Millard, S. G., Bungey, J. H., and Zhou, J. Q. (1995). "Radar assessment of structural concrete using neural networks." *NDT & E International*, 28(5), 281–288.

Nickolls, J., and Dally, W. J. (2010). "The GPU Computing Era." *IEEE Micro*, 30(2), 56–69.
Núñez-Nieto, X., Solla, M., Gómez-Pérez, P., and Lorenzo, H. (2014). "GPR Signal Characterization for Automated Landmine and UXO Detection Based on Machine Learning Techniques." *Remote Sensing*, Multidisciplinary Digital Publishing Institute, 6(10), 9729–9748.
Pasolli, E., Melgani, F., and Donelli, M. (2009). "A pattern recognition system for extracting buried object characteristics in GPR images." *2009 IEEE International Geoscience and Remote Sensing Symposium*, IV-430-IV–433.
Pasolli, E., Melgani, F., Donelli, M., Attoui, R., and de Vos, M. (2008). "Automatic Detection and Classification of Buried Objects in GPR Images Using Genetic Algorithms and Support Vector Machines." *IGARSS 2008 - 2008 IEEE International Geoscience and Remote Sensing Symposium*, II-525-II–528.
Patle, A., and Chouhan, D. S. (2013). "SVM kernel functions for classification." *2013 International Conference on Advances in Technology and Engineering (ICATE)*, 1–9.
Porsani, J. L., Ruy, Y. B., Ramos, F. P., and Yamanouth, G. R. B. (2012). "GPR applied to mapping utilities along the route of the Line 4 (yellow) subway tunnel construction in São Paulo City, Brazil." *Journal of Applied Geophysics*, 80, 25–31.
Prasad, N., Singh, R., and Lal, S. P. (2013). "Comparison of Back Propagation and Resilient Propagation Algorithm for Spam Classification." *Modelling and Simulation 2013 Fifth International Conference on Computational Intelligence*, 29–34.
Redmon, J. (2013). "Darknet: Open Source Neural Networks in C." <https://pjreddie.com/darknet/> (Sep. 7, 2020).
Redmon, J., and Farhadi, A. (2018a). "Yolov3: An incremental improvement." *arXiv preprint arXiv:1804.02767*.
Redmon, J., and Farhadi, A. (2018b). "YOLOv3: An Incremental Improvement." *arXiv*.
Rezaei, M. (2016). *Pilot Installation Report*. Edmonton, AB.
Rios, V. A. V. (2018). "Evaluation of Backfill Solution for Micro-Trenching in Cold Regions." Master of Science, University of Alberta, Edmonton, AB.
Saarenketo, T. (1997). "Using Ground-Penetrating Radar and Dielectric Probe Measurements in Pavement Density Quality Control." *Transportation Research Record*, SAGE Publications Inc, 1575(1), 34–41.
Saarenketo, T., and Scullion, T. (2000). "Road evaluation with ground penetrating radar." *Journal of Applied Geophysics*, 43(2), 119–138.
Sathya, R., and Abraham, A. (2013). "Comparison of supervised and unsupervised learning algorithms for pattern classification." *International Journal of Advanced Research in Artificial Intelligence*, 2(2), 34–38.
Shao, W., Naghdy, G., and Phung, S. L. (2007). "Automatic Image Annotation for Semantic Image Retrieval." *Advances in Visual Information Systems*, Lecture Notes in Computer Science, G. Qiu, C. Leung, X. Xue, and R. Laurini, eds., Springer, Berlin, Heidelberg, 369–378.
Shaw, M. R., Millard, S. G., Molyneaux, T. C. K., Taylor, M. J., and Bungey, J. H. (2005). "Location of steel reinforcement in concrete using ground penetrating radar and neural networks." *NDT & E International*, Structural Faults and Repair, 38(3), 203–212.
Shihab, S., Al-Nuaimy, W., and Eriksen, A. (2002a). "Image processing and neural network techniques for automatic detection and interpretation of ground penetrating radar data." *Proceedings of the 6th International Multi-Conference on Circuits, Systems, Communications and Computers, Cancun, Mexico*, 12–16.
Shihab, S., Al-Nuaimy, W., Huang, Y., and Eriksen, A. (2002b). "Neural network target identifier based on statistical features of GPR signals." *Ninth International Conference on Ground Penetrating Radar*, International Society for Optics and Photonics, 135–138.
Singh, D., and Rajan, B. (2019). "Field study on understanding effects of micro-trenching on structural performance of asphaltic pavement." *International Journal of Pavement Research and Technology*, 12(4), 435–441.

Stancu, S., Bodea, C.-N., Popescu, O. M., and Neamţu, A. (2018). "Neural Networks and their Accelerated Evolution from an Economic Analysis Perspective." *Encyclopedia of Information Science and Technology,* IGI Global, 6579–6594.

Szymczyk, M., and Szymczyk, P. (2013). "Preprocessing of GPR data." *Image Processing & Communications*, 18(2–3), 83–90.

Travassos, L. X., and Pantoja, M. F. (2019). "Ground Penetrating Radar." *Handbook of Advanced Nondestructive Evaluation*, N. Ida and N. Meyendorf, eds., Springer International Publishing, Cham, 987–1023.

Treasury Board and Finance. (2020). "Alberta population projections." Treasury Board and Finance.

United Nations. (2019). "World population prospects 2019: highlights." *Department of Economic and Social Affairs, Population Division*.

Valiati, G. R., and Menotti, D. (2019). "Detecting Pedestrians with YOLOv3 and Semantic Segmentation Infusion." *2019 International Conference on Systems, Signals and Image Processing (IWSSIP)*, 95–100.

Vapnik, V. (2000). *The Nature of Statistical Learning Theory*. Information Science and Statistics, Springer-Verlag, New York.

Vaseli, H. (2015). "Application of Micro-Trenching for Fiber to the Home." Master of Science, University of Alberta, Edmonton, AB.

Vejdannik, M., Sadr, A., de Albuquerque, V. H. C., and Tavares, J. M. R. (2018). "Signal processing for NDE." *Handbook of advanced non-destructive evaluation*.

Viola, P., and Jones, M. J. (2004). "Robust Real-Time Face Detection." *International Journal of Computer Vision*, 57(2), 137–154.

Wang, H., and Raj, B. (2017). "On the Origin of Deep Learning." *arXiv*.

Xie, X., Li, P., Qin, H., Liu, L., and Nobes, D. C. (2013). "GPR identification of voids inside concrete based on the support vector machine algorithm." *Journal of Geophysics and Engineering*, Oxford Academic, 10(3).

Youn, H., Chen, C., and Peter, L. (2003). "Automatic Pipe Detection Using Fully Polarimetric GPR." *American Society of Agricultural and Biological Engineers*, Paper No. 032343, ASAE, St. Joseph, Michigan.

Young, G. N., and Alft, K. L. (2004). "Utility mapping and data distribution system and method."

Zhang, J., Liu, Q., and Nath, B. (2004). "Landmine Feature Extraction and Classification of GPR Data Based on SVM Method." *Advances in Neural Networks*, Lecture Notes in Computer Science, F.-L. Yin, J. Wang, and C. Guo, eds., Springer, Berlin, Heidelberg, 636–641.

Zhang, J., Yang, X., Li, W., Zhang, S., and Jia, Y. (2020). "Automatic detection of moisture damages in asphalt pavements from GPR data with deep CNN and IRS method." *Automation in Construction*, 113, 103119.

Zhang, X., and Wong, W. H. (2001). "Recursive sample classification and gene selection based on SVM: method and software description." *Biostatistics Dpt. Tech Report, Harvard School of Public Health*, Citeseer.

Zhao, Z.-Q., Zheng, P., Xu, S.-T., and Wu, X. (2019). "Object Detection with Deep Learning: A Review." *IEEE Transactions on Neural Networks and Learning Systems*, 30(11), 3212–3232.

Zong, Z., Chen, C., Mi, X., Sun, W., Song, Y., Li, J., Dong, Z., Huang, R., and Yang, B. (2019). "A Deep Learning Approach for Urban Underground Objects Detection from Vehicle-Borne Ground Penetrating Radar Data in Real-Time." *ISPRS - International Archives of the Photogrammetry, Remote Sensing and Spatial Information Sciences*, 4216, 293–299.